energy&fuels

Review

pubs.acs.org/EF

Advances in Asphaltene Science and the Yen–Mullins Model

Oliver C. Mullins,*[,†] Hassan Sabbah,[‡,§,∥] Joëlle Eyssautier,[⊥] Andrew E. Pomerantz,[†] Loïc Barré,[⊥] A. Ballard Andrews,[†] Yosadara Ruiz-Morales,[#] Farshid Mostowfi,[¶] Richard McFarlane,[£] Lamia Goual,[@] Richard Lepkowicz,[$] Thomas Cooper,[%] Jhony Orbulescu,[+] Roger M. Leblanc,[+] John Edwards,[&] and Richard N. Zare[∥]

[†]Schlumberger-Doll Research, One Hampshire Street, Cambridge, Massachusetts 02139, United States

[‡]Université de Toulouse, UPS-OMP, IRAP, 31028 Toulouse Cedex 4, France

[§]CNRS, IRAP, 9 Avenue du Colonel Roche, BP 44346, 31028 Toulouse Cedex 4, France

[∥]Department of Chemistry, Stanford University, Stanford, California 94305, United States

[⊥]IFP Energies Nouvelles, 1-4 Avenue de Bois-Préau, 92852 Rueil-Malmaison Cedex, France

[#]Instituto Mexicano del Petróleo, Programa de Ingeniería Molecular, Eje Central Lázaro Cárdenas Norte 152, Distrito Federal 07730, México

[¶]DBR Technology Center, Schlumberger, 9450 17th Avenue, Edmonton T6N 1M9, Canada

[£]Alberta Innovates Technology Futures, Edmonton, Alberta T6N 1E4, Canada

[@]Department of Chemical and Petroleum Engineering, University of Wyoming, Laramie, Wyoming 82071, United States

[$]Department of Physics and Optical Engineering, Rose-Hulman Institute of Technology, Terre Haute, Indiana 47803, United States

[%]Materials and Manufacturing Directorate, Air Force Research Laboratory, Wright-Patterson Air Force Base, Ohio, 45433, United States

[+]Department of Chemistry, University of Miami, Cox Science Center, Coral Gables, Florida 33146, United States

[&]Process NMR Associates, 87A Sand Pit Road, Danbury, Connecticut 06810, United States

ABSTRACT: The Yen–Mullins model, also known as the modified Yen model, specifies the predominant molecular and colloidal structure of asphaltenes in crude oils and laboratory solvents and consists of the following: The most probable asphaltene molecular weight is ~750 g/mol, with the island molecular architecture dominant. At sufficient concentration, asphaltene molecules form nanoaggregates with an aggregation number less than 10. At higher concentrations, nanoaggregates form clusters again with small aggregation numbers. The Yen–Mullins model is consistent with numerous molecular and colloidal studies employing a broad array of methodologies. Moreover, the Yen–Mullins model provides a foundation for the development of the first asphaltene equation of state for predicting asphaltene gradients in oil reservoirs, the Flory–Huggins–Zuo equation of state (FHZ EoS). In turn, the FHZ EoS has proven applicability in oil reservoirs containing condensates, black oils, and heavy oils. While the development of the Yen–Mullins model was founded on a very large number of studies, it nevertheless remains essential to validate consistency of this model with important new data streams in asphaltene science. In this paper, we review recent advances in asphaltene science that address all critical aspects of the Yen–Mullins model, especially molecular architecture and characteristics of asphaltene nanoaggregates and clusters. Important new studies are shown to be consistent with the Yen–Mullins model. Wide ranging studies with direct interrogation of the Yen–Mullins model include detailed molecular decomposition analyses, optical measurements coupled with molecular orbital calculations, nuclear magnetic resonance (NMR) spectroscopy, centrifugation, direct-current (DC) conductivity, interfacial studies, small-angle neutron scattering (SANS), and small-angle X-ray scattering (SAXS), as well as oilfield studies. In all cases, the Yen–Mullins model is proven to be at least consistent if not valid. In addition, several studies previously viewed as potentially inconsistent with the Yen–Mullins model are now largely resolved. Moreover, oilfield studies using the Yen–Mullins model in the FHZ EoS are greatly improving the understanding of many reservoir concerns, such as reservoir connectivity, heavy oil gradients, tar mat formation, and disequilibrium. The simple yet powerful advances codified in the Yen–Mullins model especially with the FHZ EoS provide a framework for future studies in asphaltene science, petroleum science, and reservoir studies.

INTRODUCTION

The molecular and colloidal structures of asphaltenes have been the subject of extensive and lengthy investigation.[1−9] Early work led to a proposal regarding the structure of asphaltenes specifying corresponding types of chemical moieties, the "Yen model".[6] However, when this early and prescient model was proposed, major uncertainties remained about asphaltenes, including the asphaltene molecular weight, molecular architecture, aggregation species, aggregation numbers, concentration of formation,

Special Issue: Upstream Engineering and Flow Assurance (UEFA)

Received: January 31, 2012
Revised: April 16, 2012
Published: April 18, 2012

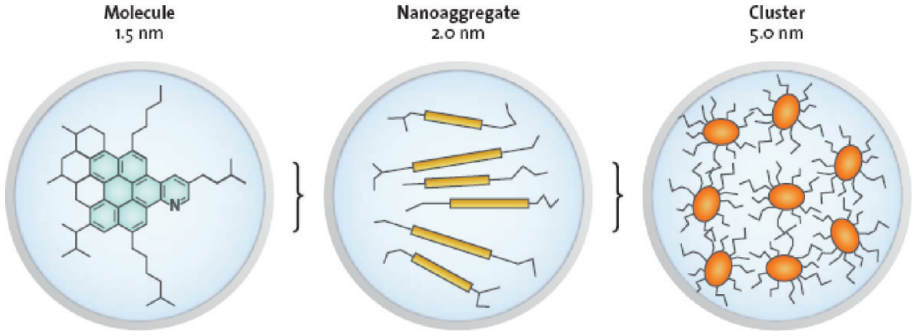

Figure 1. Yen–Mullins model.[1,2,10,11] This model shows the dominant molecular and colloidal structures for asphaltenes in laboratory solvents and crude oils. The most probable asphaltene molecular weight is ~750 g/mol (Da), and the "island" molecular architecture dominates with one aromatic ring system per molecule. With sufficient concentration, asphaltene molecules form nanoaggregates with small (<10) aggregation numbers and with one disordered stack of aromatics. At higher concentrations, nanoaggregates form clusters, again with small (<10) aggregation numbers.

and very importantly, relationship between laboratory species and those that prevail in crude oils, especially in the subsurface.[1,2] In recent years, there has been a substantial convergence of myriad data streams enabling the proposal of a much more specific model of the asphaltene molecular and colloidal structure. This model shown in Figure 1 has been called the modified Yen model[1,2] and equivalently the "Yen–Mullins model".[10,11]

Basic features of the Yen–Mullins model are evident in Figure 1. First, asphaltene molecular weights are ~750 Da, with most of the population being between 500 and 1000 Da. As previously described,[1,2] all mass spectral methods[11−16] and all diffusion measurements[17−21] now yield similar results on this topic. With this issue essentially resolved, the field could advance. The number of fused rings in asphaltene polycyclic aromatic hydrocarbons (PAHs) has been addressed by direct molecular imaging[22,23] and optical absorption and emission analysis coupled with molecular orbital (MO) calculations.[10,24,25] Raman spectroscopy also obtained similar results on asphaltene PAH size.[26] These studies indicated that the most probable number of fused rings is seven. X-ray Raman studies show that the type of aromatic carbon that dominates asphaltenes is the more stable "sextet" carbon and not the isolated double bond.[27] Chemical stability is not a surprising attribute of asphaltenes. However, nuclear magnetic resonance (NMR) studies indicated that substantially smaller PAHs dominated asphaltenes;[28] thus, uncertainty exists here and merits closer investigation.

For the known asphaltene molecular weights, only one PAH of seven rings can comfortably fit within this constraint, the so-called island architecture. The first studies that proposed the island architecture were the time-resolved fluorescence depolarization (TRFD) studies.[17,18,29,30] These nondestructive studies indicate that, in asphaltenes, blue-fluorescing chromophores rotationally diffuse 10 times faster than red-fluorescing chromophores and, thus, are not cross-linked. Several destructive studies involving unimolecular fragmentation of asphaltenes and model compounds also obtained unambiguous evidence of island molecular architecture of asphaltenes.[11,31] However, bulk decomposition studies of asphaltenes appeared to indicate the predominance of smaller ring systems;[32] therefore, asphaltene molecular decomposition merits a closer look. If asphaltene PAHs have fewer than seven fused rings, then more than one ring system can be compatible within the molecular-weight constraint. When much larger asphaltene molecular weights were considered correct, molecular structures were proposed with many PAHs per asphaltene molecule, the so-called archipelago model. The name has been retained even for proposed molecular structures with only two PAHs. Indeed, if two asphaltene PAHs are directly bonded via a single bond, then optical methods, such as TRFD, might still identify this as a single chromophore, thereby blurring the distinction between island versus archipelago. In addition, some decomposition studies find this single bonded pair of PAHs as a single entity as well. In addition, the TRFD studies noted that a small fraction of asphaltene molecules might have two PAHs in a single molecule.

In general, the various results associated with asphaltene nanoaggregates and clusters have not been the subject of as much debate as molecular properties, with the exception of the critical nanoaggregate concentration (CNAC). Fluorescence methods showed that asphaltene molecules in toluene associate at low concentrations (~50 mg/L).[33] The first correct measurement of asphaltene CNAC was by high-Q ultrasonic measurements,[34] essentially measuring the change of solution compressibility upon aggregation. The measured CNAC is ~100 mg/L. While this result is 20 times lower in concentration than previous studies, it was quickly confirmed by alternating-current (AC) conductivity,[35] direct-current (DC) conductivity,[36,37] NMR hydrogen index,[21] NMR diffusion,[21] and centrifugation (both live oil[38] and toluene solutions[39]). Small-angle X-ray scattering (SAXS) and small-angle neutron scattering (SANS) have provided a wealth of information regarding asphaltene nanostructures.[40−46] All studies show nanocolloidal species; nevertheless, the specific results are somewhat model-dependent. X-ray scattering is dependent upon electron density and, thus, is induced primarily by carbon in asphaltenes, in particular aromatic ring systems. On the other hand, neutron scattering is dependent upon hydrogen nuclei, in particular alkanes in asphaltenes. By contrasting absolute cross-sections of SAXS versus SANS, one has a measure of the different spatial distributions of aromatic carbon versus alkane groups in asphaltenes. In this way, it was shown that asphaltene nanoaggregates have a single stack of PAHs in the interior with alkanes on the exterior,[45,46] essentially consistent with the picture shown in Figure 1. These studies also obtained the larger colloidal particles, the clusters.[45,46]

Oilfield studies have also provided a stringent test of the colloidal structure of asphaltenes.[47] In particular, for low gas-to-oil ratio (GOR) black oils, the gravity term dominates for producing asphaltene gradients. Thus, the measurement of these gradients gives the size of asphaltene particles directly. The first study of this kind obtained nanoaggregate sizes compatible with Figure 1. Subsequent refinements with application to nanoaggregates in

dx.doi.org/10.1021/ef300185p | Energy Fuels 2012, 26, 3986−4003

reservoir black oils[47] and clusters in reservoir heavy oils[2] have reinforced the Yen–Mullins model.

Nevertheless, uncertainties persist in the field of asphaltene science. The molecular architecture and PAH ring size remain subjects of debate. Both nanoaggregates and clusters are very small and formed in solvent systems that provide only small contrast to the colloidal asphaltenes. Indeed, there appears to be no single methodology that provides complete and definitive characterization of these species. It is preferred to treat the many different studies in terms of a single framework, if applicable. In this report, we provide a view of many recent studies in asphaltene science, particularly from the vantage of the Yen–Mullins model. Asphaltene decomposition studies have been the backdrop of seemingly contradictory results. Recent work has resolved this to a significant extent, particularly through the use of model compounds. The canonical optical properties of asphaltenes, particularly their color, relate to their PAH distribution and have been investigated in stringent new ways involving both theory and experiment associated with triplet-state transitions. Uncertainties in the application of NMR to asphaltenes have been clarified. New comparative studies on nanoaggregate formation and cluster formation have been tested by very different physics. Length scales have been tested by atomic force microscopy (AFM). Powerful new SAXS and SANS studies have provided an excellent test of the Yen–Mullins model. Oilfield studies reinforce this nanoscience model and obtain intriguing results in accordance with basic features and even subtleties in the SAXS and SANS results. To be clear, in all cases, the Yen–Mullins model is reinforced. A new and powerful theoretical formalism, the Flory–Huggins–Zuo equation of state (FHZ EoS), has been founded on the Yen–Mullins model and is proving very valuable to address myriad fluid complexities previously unaccounted for in oilfield reservoirs.

■ ASPHALTENE MOLECULAR ARCHITECTURE

Two-Step Laser Desorption Ionization Mass Spectrometry (L^2MS). The topic of asphaltene molecular architecture is difficult to address. Asphaltenes are chemically polydisperse, and as is the case with many properties, one might be interrogating a subset of asphaltene molecules. The nondestructive technique TRFD diffusion measurements applied to asphaltenes show blue chromophores rotationally diffuse 10 times faster than red chromophores. Thus, the different chromophores are not cross-linked. Nevertheless, the interrogated molecules must fluoresce. Other methods must be used to investigate this issue. L^2MS has been used to probe asphaltenes.[11,48−50] In general, because of the convenient laser wavelength selection, L^2MS methods are sensitive to molecules with one or more PAHs. This is not much of a limitation. The dependence of ionization cross-section upon specific PAHs has been investigated. While there is some variability dependent upon specific laser wavelengths chosen, L2MS methods applicable to asphaltenes have a smaller than a factor of 4 variation in cross-sections for various PAHs.[11,48−50] Given the large number of PAHs in asphaltenes, these differences likely average out.

A schematic of the technique is shown in Figure 2.

Figure 3 shows that L^2MS avoids interference from molecular aggregation that can be dominant in laser desorption ionization (LDI) mass spectra. Here, the L^2MS and LDI spectra of gentisic acid (2,5-dihydroxybenzoic acid) are contrasted. Gentisic acid is a standard matrix used in matrix-assisted LDI.[48] LDI is also seen to yield fragmentation, while L^2MS does not.[48] For asphaltenes, with

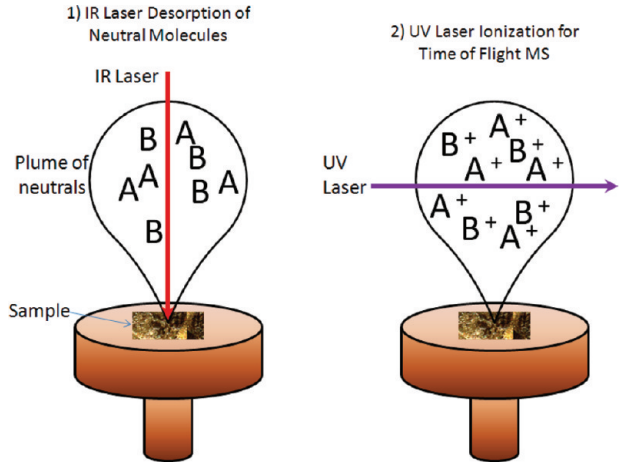

Figure 2. Schematic of the process in L^2MS. The IR laser desorbs the sample, yielding a neutral plume. The UV laser ionizes the sample, enabling time-of-flight mass spectrometry analysis.[11,48−50]

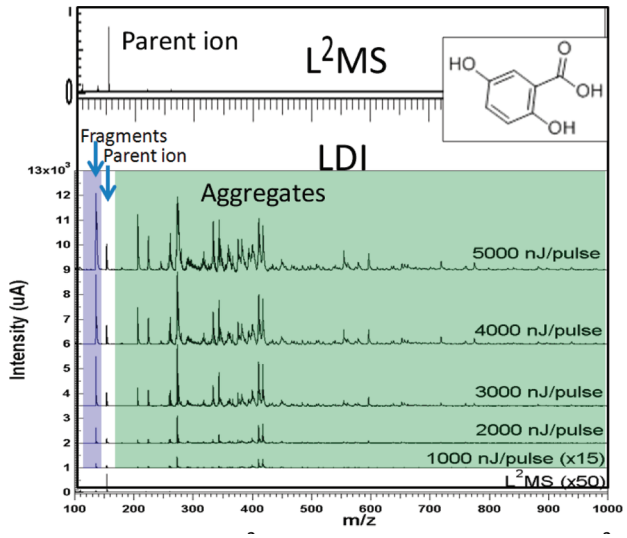

Figure 3. Contrast of L^2MS versus LDI mass spectra. L^2MS (top and bottom) gives predominantly the parent ion without being subject to molecular aggregation effects nor much fragmentation. LDI (middle five spectra with shaded regions) suffers from much more aggregation and also fragmentation.[48]

their propensity for aggregation, it is important to attempt to minimize these effects with chosen methods of investigation.

L^2MS applied to asphaltenes[11,49,50] gives molecular-weight distributions shown in Figure 4 and is similar to other mass spectra results and diffusion studies for asphaltenes.[1,2] The asphaltene mass distribution in L^2MS spectra are not sensitive to the power of either laser, the surface asphaltene concentration, or the time between laser pulses, yielding a robust result.

L^2MS can also be used to probe molecular architecture augmented by the lack of aggregation effects evident in Figures 3 and 4. Figure 5 shows that, in L^2MS, molecular fragmentation can be made to occur in some cases.[11] Only a few specific examples are shown in Figure 5. Reference 11 provides much more detail on the 23 island and archipelago compounds that were analyzed. Specifically, archipelago model compounds that have two PAHs connected by an alkane bridge are seen to be unstable to fragmentation, especially at higher laser powers, while island molecular architectures with pendant alkanes on a

dx.doi.org/10.1021/ef300185p | Energy Fuels 2012, 26, 3986−4003

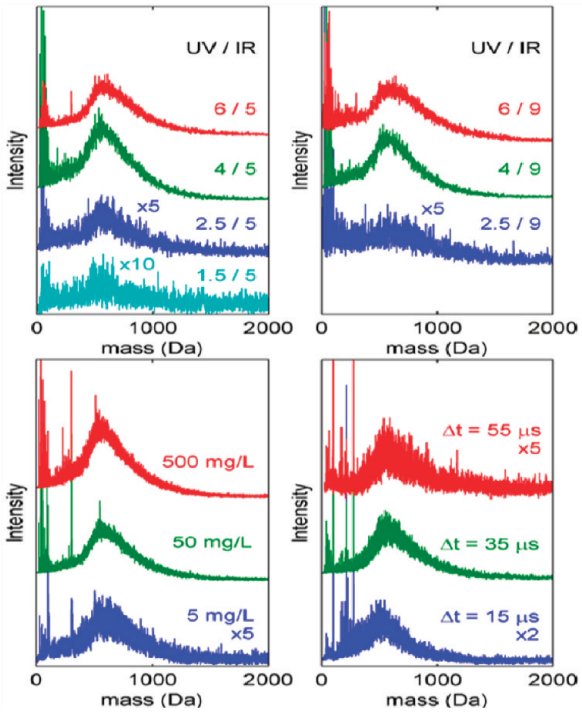

Figure 4. L^{2}MS on asphaltenes yielding a robust molecular-weight distribution independent of the power of either laser (top spectra), surface asphaltene concentration (bottom left spectra), or time of ion collection (bottom right spectra).[50]

single PAH are much more resistant to fragmentation.[11] The instability of archipelago compounds in L^{2}MS is dependent in part upon the ionization method. With multiphoton ionization, the archipelago compounds can be stabilized to a degree by alkyl substitution. Nevertheless, in all cases, the archipelago model compounds were less stable than the island model compounds. In the latest work using laser desorption, single photon ionization mass spectrometry, a single, high-energy ultraviolet (UV) photon is used for ionization.[11] For single-photon ionization, no enhancement of stability from alkyl substitution was seen for archipelago compounds. In these L^{2}MS experiments, the instability of archipelago model compounds versus the stability of asphaltenes and island compounds presents a strong case for the dominance of the island molecular architecture for asphaltenes.[11,48]

To explore the implications of the asphaltene molecular architecture, the L^{2}MS spectra of 23 model compounds, both island and archipelago, are compared to corresponding spectra of asphaltenes. Figure 6 shows this comparison under conditions of increasing ionization laser power.

The L^{2}MS results shown in Figure 6 indicate that asphaltenes are stable with respect to fragmentation, as are all of the island model compounds examined here.[11] Asphaltenes live for geologic time; thus, stability is expected. Olefins, especially vinyl olefins, tend to be unstable and are typically not found in reservoir crude oils unless there are special circumstances.[51] Indeed, olefins are often obtained in considerable quantity in laboratory cracking of kerogen, especially in anhydrous conditions.[52] However, when the laboratory cracking of kerogen is carried out over a 6 year time span even with relatively anhydrous conditions, olefins are not found in the resulting hydrocarbons presumably because of their instability.[52] Laboratory thermal processes gives rise to olefins[52] and to archipelago compounds[53] as discussed below, yet crude oils and asphaltenes evidently lack any appreciable concentration of these relatively unstable compounds.

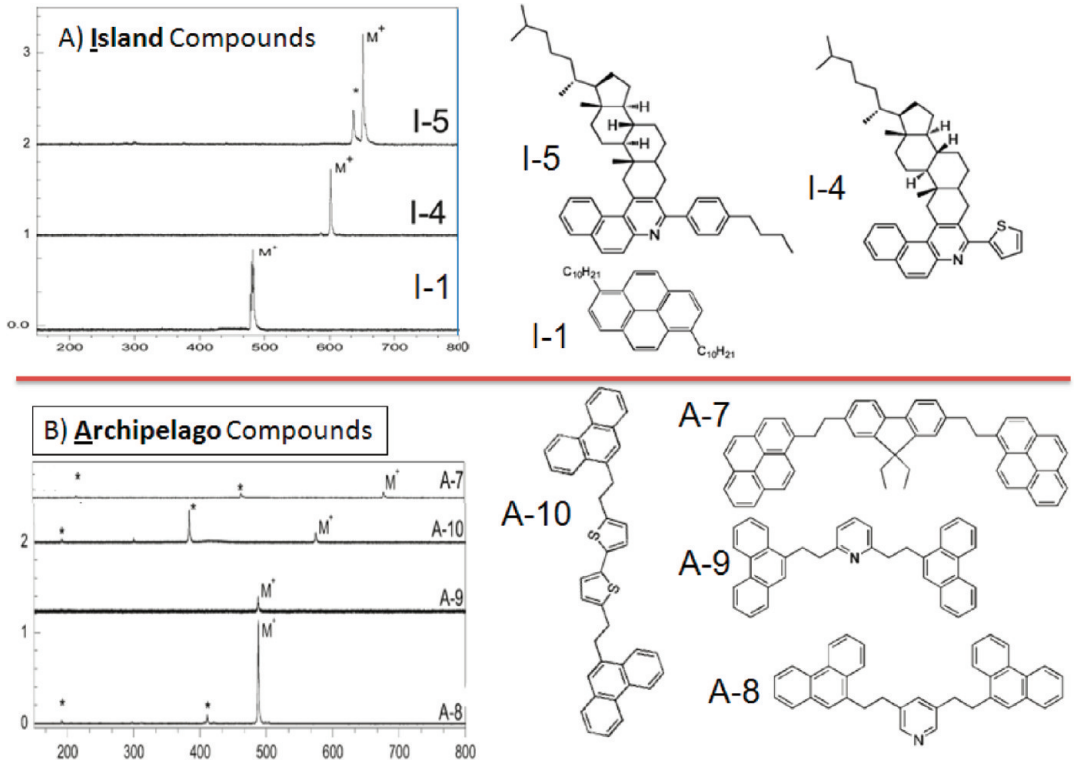

Figure 5. L^{2}MS applied to asphaltenes and model compounds (structures on right) with island (top) and archipelago (bottom) structures. The archipelago molecules are subject to more fragmentation than the island compounds for similar experimental conditions.[11] The asphaltenes behave in the same way as the island compounds and not as the archipelago compounds behave.

dx.doi.org/10.1021/ef300185p | Energy Fuels 2012, 26, 3986−4003

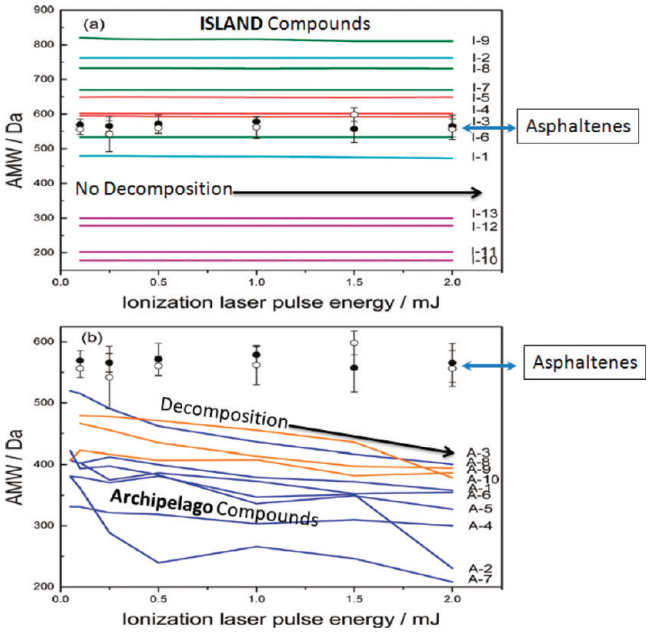

Figure 6. The apparent average molecular weight (AMW) versus ionization laser power obtained from L^2MS spectra of 23 model compounds and asphaltenes.[11] With fragmentation, the AMW of the *y* axis decreases. This plot shows that, under the same conditions, none of the island model compounds fragments, while all of the archipelago model compounds fragment. The asphaltenes do not fragment. The implication is that asphaltenes are predominantly island architecture.[11] The chemical stability of asphaltenes shown here is expected because they live for geologic time.

The L^2MS experiments shown in Figure 6 correspond to unimolecular decomposition. Some bulk decomposition experiments of asphaltenes have been interpreted as being consistent with the archipelago molecular architecture.[32] However, it has recently been established that bulk decomposition of various model compounds results in copious synthesis of archipelago compounds.[53] Specifically, pyrolysis of island model compounds yields archipelago compounds for up to $^1/_2$ of the sample. These bulk decomposition studies are very important for understanding molecular structures formed in processing these materials.[53] However, it appears evident that this result precludes any significant utility of bulk pyrolysis of asphaltenes for distinguishing initial asphaltene molecular architecture. Indeed, decomposition energies exceed reaction temperatures; therefore, this result is not altogether surprising. The pyrolysis study did declare that the ease of forming archipelago compounds was a strong argument for the existence of a substantial archipelago component in asphaltenes. Still, the specifics of the thermal process might control the extent of archipelago formation. Moreover, we caution that, as with olefins, it is not the formation of chemical species (only) but rather their stability that can dominate in determining the bulk composition of crude oils and, thus, asphaltenes. Figure 6 indicates that archipelago compounds are unstable and could explain the evident dominance of island compounds in asphaltenes. If petroleum samples are subject to significant chemical reaction, then different species could be found.

Other unimolecular decomposition studies have recently been reported for asphaltenes from virgin crude oil, with "virgin" meaning unaltered by any process, such as thermal decomposition of refining. Laser-induced acoustic desorption (LIAD) mass spectrometry using electron impact ionization has been reported. Archipelago model compounds were shown to undergo large mass loss upon fragmentation, while asphaltenes and island model compounds showed much smaller mass loss. The corresponding products from decomposition tend to have small mass loss, which is consistent with the loss of alkane groups from island compounds (as opposed to splitting the compounds in half for two PAHs bridged by an alkane linkage).[54] In another LIAD study, a specific compound was identified, naphthylnaphthalene in asphaltene.[55] For reasons unknown, there was no phenylnaphthalene detected nor biphenyl nor other compounds that one might consider as plausible as naphthylnaphthalene in asphaltene.[55] This compound was identified as an "archipelago" compound. We note that, from an optical standpoint, naphthylnaphthalene would appear as a single chromophore and falls within the single PAH classification as far as the TRFD experiments are concerned. Such compounds consisting of direct linkages of PAHs might be considered to fall within an overlap of island versus archipelago molecular architecture.

SIZE OF ASPHALTENE PAHS

PAH Size: Singlet- and Triplet-State Spectroscopies. The size of asphaltene PAHs remains of interest, and several recent studies have addressed this question. One study of a notable blue crude oil, a light crude oil, identified a five-ring PAH perylene as the source of the blue color.[56] Figure 7 shows this oil. The figure also shows the two-dimensional fluorescence spectra of this oil and perylene.[56] This spectral comparison is one of several methods that identified perylene as dominating the blue color (fluorescence) of this crude oil. The relationship between optical properties and PAHs is clearly established here. Moreover, finding a five-ring PAH in a light crude oil helps guide thinking into the types of PAHs that can arise in much heavier oils and asphaltenes.

Indeed, the deep brown color of asphaltenes is one of their canonical properties and is consequently quite useful to characterize asphaltene PAHs. By and large, there is no disagreement among asphaltene researchers about the optical absorption or fluorescence emission properties of asphaltenes. Interpretation of these properties mandated an exhaustive molecular orbital study, which reinforced a simple picture.[24,25] For example, small PAHs are colorless and cannot account for asphaltene color. Previous studies focused on the electronic spin-singlet manifold, for both absorption and emission.[24,25] These studies have now been extended to include the electronic spin-triplet manifold as well.[57] For a population distribution of PAHs, singlet-state spectra differ substantially from triplet-state spectra obtained by pump–probe experiments, thus providing a stringent test relating presumed PAH distributions of asphaltenes with optical spectra.

Triplet-state spectra of asphaltenes and crude oils were obtained with the optical pump–probe system shown in Figure 8. Figure 9 shows the processes involved and asphaltene spectra obtained in both the ground state (dominated by spin singlets)[24,25] and the triplet excited state.[57]

A strong pulse at 355 nm excited the ground state for dilute solutions of the selected sample. At a specified time later, a flash lamp was used to obtain the spectrum. When the spectrum is measured with and without the pump laser, the differential absorption of the triplet state can be measured. These experiments rely on the much longer lifetime of triplet states than excited singlet states. The so-called "hole burning" is evident in the triplet spectrum (right in Figure 9). After the strong 355 nm pulse, there is a depletion of population that absorbs at 355 nm.

dx.doi.org/10.1021/ef300185p | *Energy Fuels* 2012, 26, 3986–4003

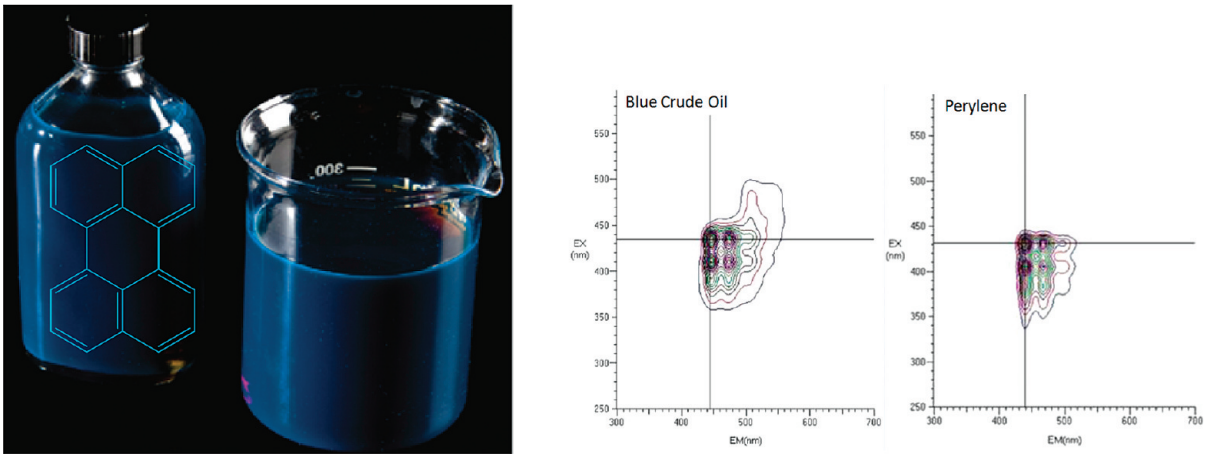

Figure 7. (Left) Light crude oil from deep water, Gulf of Mexico. Its unusual blue color is due to fluorescence from a specific component, perylene (molecular structure shown). (Right) Two-dimensional fluorescence spectra identify perylene as dominating the blue fluorescence emission from this crude oil.[56]

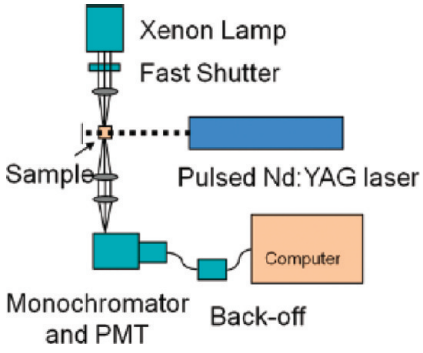

Figure 8. Pump−probe system used to obtain triplet-state spectra of asphaltenes and crude oils.[57] The 355 nm laser line from the Nd:YAG laser excited the ground state. Triplet-state spectra are then measured with the Xe flash lamp. A schematic of the process is shown in Figure 9.

Consequently, the pump−probe absorbance at 355 nm is less than absorption without the pump, and a negative absorption results, as shown in the triplet-state absorption (right in Figure 9).

For the following, we presume the asphaltene PAH distribution that accounts for the singlet manifold optical data (left in Figure 9) and determine whether this is consistent with the triplet manifold data (right in Figure 9). The corresponding PAH distribution is centered at seven fused rings and symmetrically falls off with equal populations of six fused rings, eight fused rings, etc. In the pump−probe experiments, the 355 nm excitation can excite the first and higher lying excited singlet states with strong electronic transitions of populous PAHs in asphaltenes. Figure 10 shows that this corresponds to PAHs with five, six, and seven fused rings. The weak flash lamp probe excites predominantly the first excited triple state of these PAHs (right in Figure 10). These triplet-state theoretical curves are very red-shifted, with maxima at 700 nm, compared to the ground (singlet) state absorption at the original pump laser at 355 nm (cf. Figure 10). Indeed, this is exactly what is observed in the pump−probe experiment for asphaltenes (right in Figure 9).[57]

Part of the large red shift of the triplet states is due to excitation of higher lying excited singlet states by the powerful pump pulse. The lack of small ring systems in asphaltenes guarantees that much of the short wavelength optical absorption will occur in larger PAHs with lower energy transitions. Indeed, pump−probe experiments on crude oils showed much smaller red shifts in the triplet manifold, reflecting the presence of small PAHs in crude oils with their higher energy transitions.[57] Correspondingly, the triplet-state spectra for asphaltenes in Figure 11 show much larger red shifts than the triplet-state spectra for crude oil. Pauli exclusion is also responsible for part of the red-shifted triplet spectra for both crude oils and asphaltenes. The triplet-state electrons are in the same spin state and, thus, cannot have the same orbital quantum numbers. Consequently, the lowest triplet state has one electron with a higher principal quantum number and, therefore, with smaller excitation energies, as mandated by the Rydberg equation. Pauli exclusion explains much of the red shift of the triplet-state spectrum of crude oil compared to the 355 nm pump seen in Figure 11.

The salient feature of the pump−probe experiments of asphaltenes along with the comparison to theory is that the very different asphaltene spectra in the singlet-state versus triplet-state manifold are consistent with an asphaltene PAH population centroid at seven fused rings and largely rule out dominance of small PAHs in asphaltenes.[57] Asphaltenes are strongly colored in the visible spectrum, and their UV absorbance is not orders of magnitude higher in sharp contrast to absorption spectra observed for small PAHs. As a final note, various other measurements were performed in the pump−probe experiments to validate that indeed triplet-state measurements were being performed. This included measurements of quenching by different concentrations of molecular oxygen and temperature effects on quenching rates that gave Arrhenius activation energies for quenching. All measurements are consistent with the explanations above.[57]

PAH Size: NMR. Many different lines of investigation are in accordance with the fact that the most probable number of fused rings in asphaltene PAHs is approximately seven. In addition to the above, direct molecular imaging by both scanning tunneling microscopy[22] and high-resolution transmission electron microscopy[23] gives this result. An early NMR study came to the same conclusion.[58] Rotational diffusion studies by TRFD obtained similar diffusion constants for seven fused ring PAHs with alkyl substituents and asphaltenes.[17,18,29,30]

However, one study is at odds with these other studies. A ^{13}C NMR study was performed and obtained PAHs of two, three, and four fused rings for asphaltenes.[28] The study used single-pulse excitation (SPE) to obtain ^{13}C NMR spectra. A spectral cutoff between protonated and nonprotonated aromatic carbon

dx.doi.org/10.1021/ef300185p | Energy Fuels 2012, 26, 3986−4003

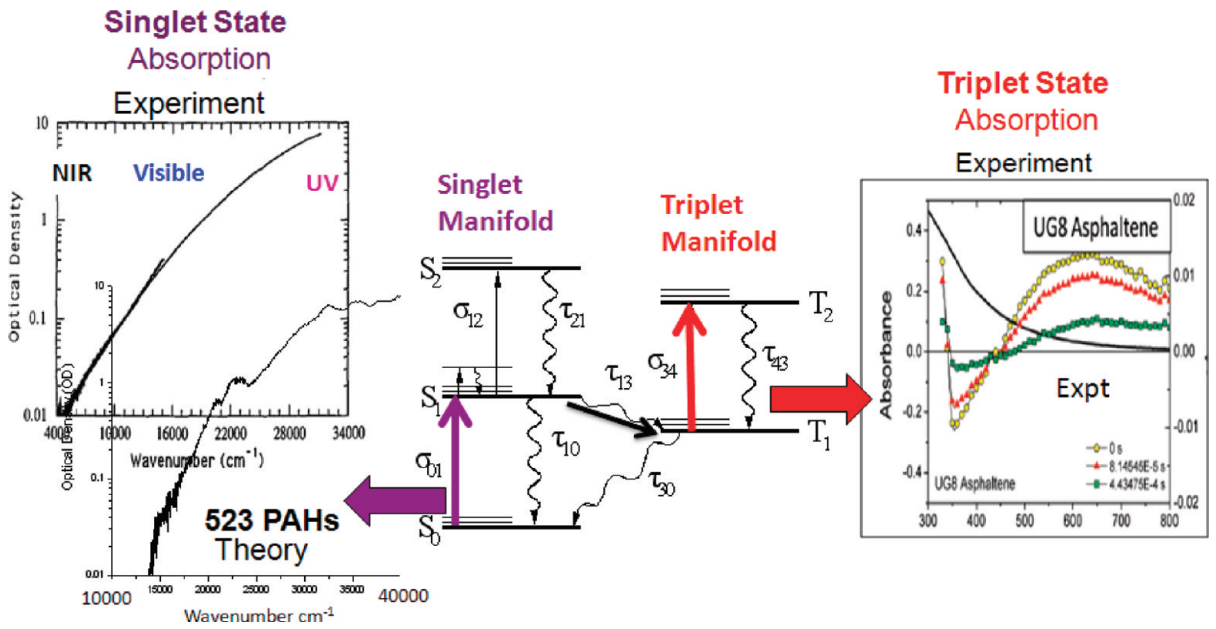

Figure 9. (Left) Singlet manifold absorption asphaltene spectra, both experiment (top) and theory (bottom).[57] The theoretical curve presumes an asphaltene PAH distribution centered at seven fused rings. (Right) Triplet manifold absorption spectra (versus time delay) of asphaltenes using a 355 nm laser pump to excite the ground singlet state S_0. (Middle) After excitation, intersystem cross causes population of the triplet state T_1. A subsequent flash lamp pulse excites the triplet. The difference in absorption with and without the pump 355 nm laser is plotted.

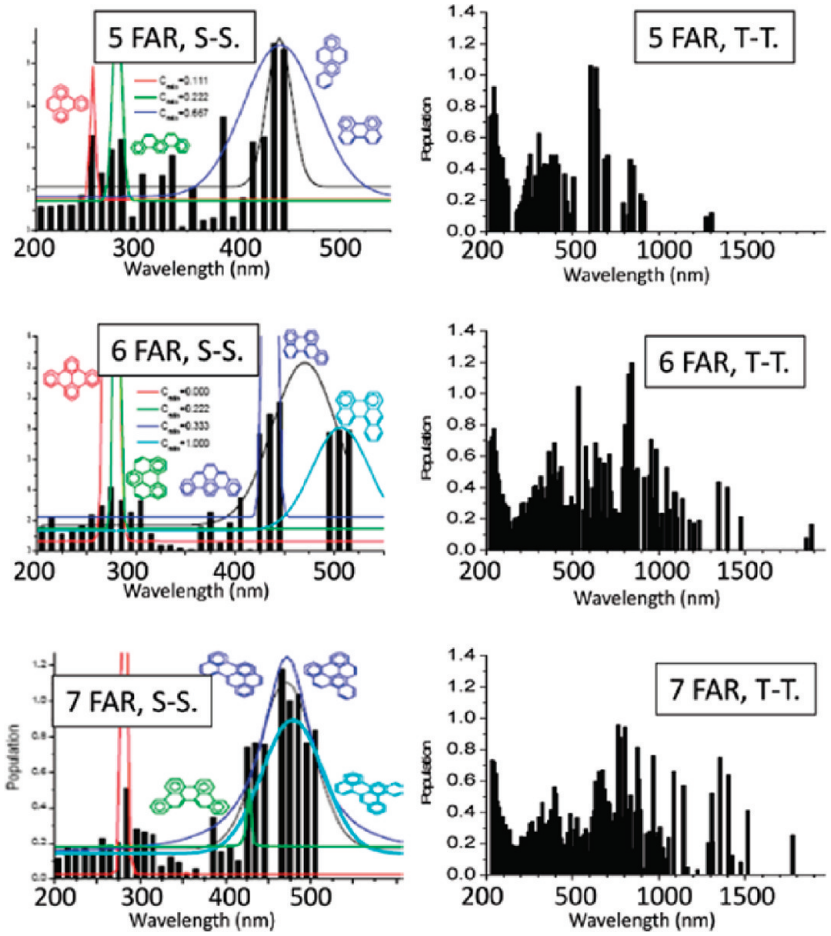

Figure 10. Molecular orbital calculations obtained for large numbers of PAHs with five, six, and seven fused aromatic rings. (Left) Singlet−singlet (S−S) transition spectra. (Right) Triplet−triplet (T−T) transition spectra. Note the large red shift obtained for triplet-state spectra.[57] This large red shift is consistent with the triplet-state spectra in Figure 9.

dx.doi.org/10.1021/ef300185p | *Energy Fuels* 2012, 26, 3986−4003

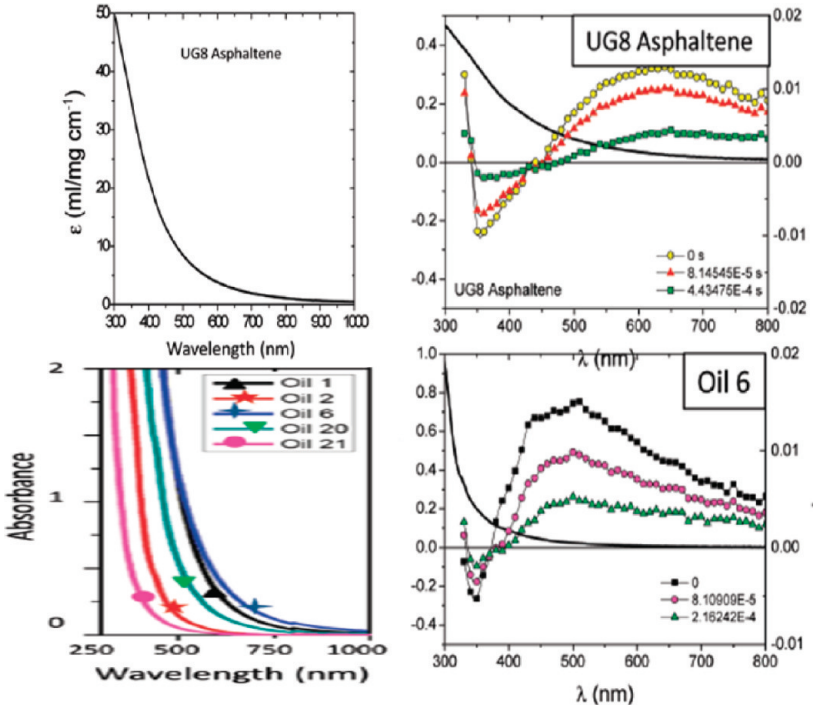

Figure 11. Optical absorption spectra. (Left) Ground-state absorption spectra. (Right) Triplet-state spectra from pump−probe experiments. (Top) Asphaltenes. (Bottom) Crude oil. The much larger red shift (versus 355 nm pump laser) of the triplet-state spectra of asphaltenes versus crude oils is due to the lack of small PAHs in asphaltenes. The results are consistent with asphaltene PAH distribution centered at seven fused rings.[57]

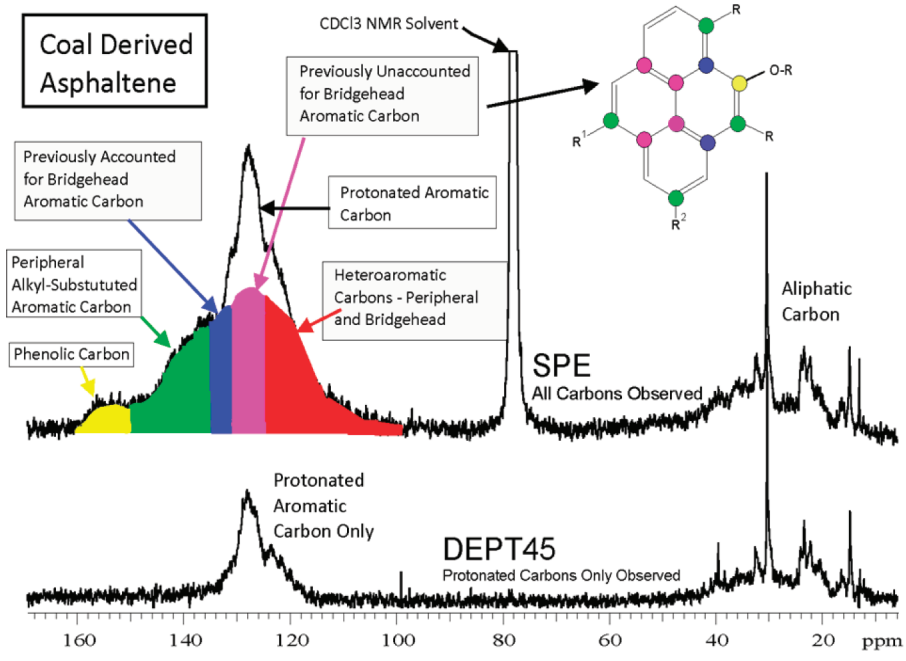

Figure 12. Comparison between DEPT and SPE ^{13}C NMR spectra of a coal-derived asphaltene.[59] The DEPT spectrum obtains protonated aromatic carbon. The SPE spectrum shows all aromatic carbon. Bridgehead carbon is a very important difference.[59] This study reveals bridgehead carbon that was likely missed by a previous NMR study (see ref 28). Undercounting bridgehead carbon leads to low estimates for the number of fused rings.

was selected (130 ppm) and used to estimate bridgehead versus peripheral aromatic carbon, thereby one can obtain estimates of the number of fused rings in a PAH (knowing that there is peripheral carbon in the 133−150 ppm range).[28] In short, this study concluded that there is only a small fraction of bridgehead carbon; thus, the conclusion was reached that asphaltene PAHs are small.[28] However, these simple integration calculations performed on ^{13}C SPE spectra suffer from the almost complete overlap of protonated and nonprotonated carbon signals in the 108−129.5 ppm region of the spectrum, leading to underestimation of the nonprotonated carbon content that occurs using such traditional chemical-shift region integrations.

Recently, a more rigorous NMR approach was used to investigate this same question of bridgehead to peripheral carbon, and a very different conclusion was obtained.[59] Indeed, the new NMR study is in close accordance with the previous studies,

dx.doi.org/10.1021/ef300185p | Energy Fuels 2012, 26, 3986−4003

yielding ~7 PAHs in virgin petroleum asphaltenes, with ~6 PAHs in coal-derived asphaltenes.[59] This NMR study provided direct interrogation of aromatic carbon bonded to hydrogen as opposed to assigning a spectra cutoff. The corresponding method is distortionless enhancement by polarization transfer (DEPT) NMR. When DEPT ^{13}C NMR spectra are compared to SPE spectra, one directly determines aromatic carbon with hydrogen. Figure 12 shows the corresponding spectra for a coal-derived asphaltene.

Figure 12 shows ^{13}C NMR data acquired for coal-derived asphaltenes. This choice of sample was partly motivated by the very small alkane fraction of coal-derived asphaltenes,[29] because of both the lack of alkane in coal and the loss of alkane in refining coal-derived liquids, with the process leading to resid and, thus, these coal-derived asphaltene samples. The lack of much alkane substitution on the PAHs of coal-derived asphaltenes simplifies the analysis, validating the DEPT and SPE ^{13}C NMR spectral comparison. Further simplification with coal-derived asphaltenes results from their being roughly $^1/_2$ of the molecular size of petroleum asphaltenes because of primarily the lack of the large alkane component in petroleum asphaltenes and, secondarily, the somewhat smaller PAH.[19,29,60] The ~50% mass fraction of alkane carbon on petroleum asphaltenes includes many long chains. The ~17% mass fraction of alkane carbon in coal-derived asphaltenes is in short chains.[29,59]

Previous NMR studies[61] of asphaltenes from virgin crude oils also found PAHs with 5−10 fused aromatic rings, thus, almost identical results to those obtained from the ^{13}C DEPT study.[59] Moreover, this previous NMR study[61] explicitly noted that they obtained similar diffusion constants for asphaltene molecules as the TRFD study (see ref 17 herein) and the fluorescence correlation spectroscopy (FCS) study referenced herein (see ref 20 herein). This NMR[61] work also found clear evidence of nanoaggregates[61] but did discuss variations in their nanoaggregates, which are not consistent with reports herein. These variations were attributed to the presumed variations in the molecular architecture also not observed herein. Nevertheless, the overall agreement on the major asphaltene issues of PAH size, molecular diffusion constants, and existence of nanoaggregates is encouraging.[61] A NMR study was also performed on resid asphaltene.[62] This study noted that the process of refining cracks alkanes off PAH cores significantly, modifying the molecular architecture of alkyl aromatics.[62] As noted above and elsewhere,[1] this process results in smaller asphaltene PAHs. The resulting resid asphaltenes were evaluated to have PAHs with four fused rings on average.[62] This represents a lower limit for virgin crude oil asphaltenes. In addition, this paper postulates the existence of some archipelago molecular architecture in addition to island molecular architecture for asphaltenes.[62] It has recently been shown that archipelago molecular architecture is produced in the thermal processing of these materials.[53]

Coal-Derived versus Petroleum Asphaltenes. The perspective is reinforced that simple heuristics are useful to account for differences observed for asphaltenes from different sources.[1,2,29,50,59,63,64] In general, the single PAH core in asphaltene molecules is the primary site of intermolecular attraction because of both its polarizability and some degree of charge separation associated with heteroatoms in the aromatic ring system, such as nitrogen. The peripheral alkane substituents yield steric repulsion, inhibiting molecular association. With the attractive forces in the molecular interior and the repulsive forces on the molecular exterior, small aggregation numbers are predicted for nanoaggregates, as discussed below. In contrast, an archipelago architecture would give multiple binding sites in single molecules, leading to gel formation at low concentrations. This is never observed for asphaltenes.

Asphaltenes are defined by their solubility classification. The repulsive and attractive intermolecular forces must balance. A decrease in alkane substitution must lead to a corresponding decrease in PAH ring size. Coal-derived asphaltenes have much less alkane than petroleum asphaltenes. First, coal-derived asphaltenes are from coal that lacks much alkane. Second, coal-derived asphaltenes are from coal liquids that were subject to vacuum distillation. This thermal process cracks off alkane substitution from PAHs. Thus, coal-derived asphaltenes are much lower in molecular weight and also have smaller PAHs than petroleum asphaltenes.[29,50,59] Petroleum resid asphaltene with its reduced alkane content also exhibits reduced PAH size.[63] Initial asphaltene molecules that are subject to alkane removal by cracking in distillation become less soluble forming coke. This molecular population with larger PAHs is thus removed from the asphaltene fraction.

For coal-derived asphaltene, most of the heteroatom content is lost in the hydrogenation to form coal liquids and subsequent vacuum distillation; thus, the differences between coal-derived asphaltenes and petroleum asphaltenes are not dominated by heteroatom concerns.[29,59]

■ NANOAGGREGATES AND CLUSTERS

Many of the techniques that are sensitive to the colloidal properties of asphaltenes provide information on both nanoaggregates and clusters. Relevant issues for these nanocolloidal particles are the concentration of formation and aggregation number (or size). For the different investigative methods, more robust results are often obtained for either the concentration of formation or the aggregation number but generally not both.

CNAC. The CNAC of asphaltenes has recently been addressed by both by DC conductivity measurements and centrifugation of asphaltene−toluene solutions. Of the many techniques that have been used to investigate CNAC of asphaltenes in toluene, perhaps DC conductivity is the most robust. However, DC conductivity is sensitive to the very small mass fraction of asphaltene molecules that are charged in toluene solution, on the order of 10^{-4} or less.[36,65] Consequently, it is important to check whether DC conductivity results for CNAC agree with other methods sensitive to the entire sample, but that may be more difficult to analyze quantitatively. It has already been shown that DC conductivity gives the same CNAC results as high-Q ultrasonic spectroscopy for the same asphaltene samples.[36] A recent study showed that the CNAC obtained by DC conductivity matched that obtained by centrifugation for the same asphaltene.[65] Centrifugation provides unassailable evidence that there is an increase in aggregation at the CNAC, the same CNAC obtained by DC conductivity. The latter technique provides a close look at the concentration of the CNAC but only by analysis of a small subset of asphaltenes.[65] These two different techniques are very complementary and support all previous studies on CNAC. Figure 13 shows the DC conductivity and centrifugation results.[65] The small change of the Stokes drag upon aggregation (small reduction in conductivity at CNAC) indicates that the nanoaggregates are small. Moreover, the centrifugation experiments were designed to collect small nanoaggregates.[65] Both of these experiments are consistent with small aggregation numbers of asphaltene nanoaggregates.

In Figure 13, the development of a concentration gradient is very clear at 100 mg/L. The absence of the concentration gradient at 50 and 75 mg/L is also equally clear.[65] We emphasize that, within measurement error, there is no gradient at these lower concentrations but a strong and clear gradient at 100 mg/L. This is consistent with the abrupt appearance of aggregates

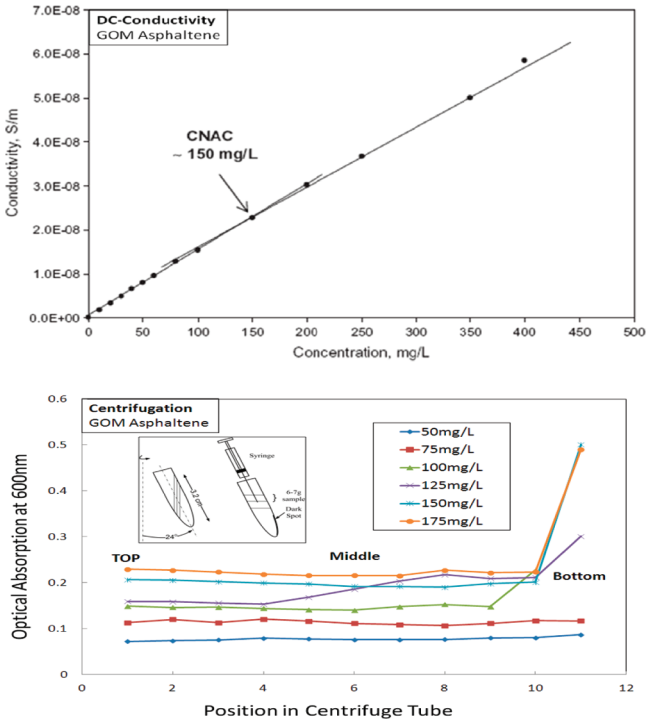

Figure 13. Comparison of DC conductivity (top) and centrifugation (bottom) applied to a specific Gulf of Mexico (GOM) asphaltene shows excellent agreement of the measured CNAC.[65] At 150 mg/L asphaltene in toluene, the DC conductivity plot shows a reduction of conductivity associated with increased Stokes drag upon aggregate formation. The centrifugation plot shows a significant increase in collected asphaltene at the base of the centrifuge tube at 150 mg/L for this asphaltene.[65] Below 75 mg/L, there is no measured gradient. At 100 mg/L, there is a substantial gradient showing an abrupt change in aggregation.

between 75 and 100 mg/L, which are significantly larger than those present at or below 75 mg/L because all of the solutions were allowed to settle simultaneously under the same conditions. Because the concentration gradient appeared abruptly at concentrations at or above 100 mg/L and is not even weakly observed at a concentration at or below 75 mg/L, we believe that a concentration of roughly 100 mg/L must represent a critical concentration for the appearance of a gradient in the settled fluid because of an abrupt change in the aggregation state in this concentration range.[65] As discussed previously, there is a range of concentrations for critical concentrations, such as CNAC or critical micelle concentration, with a small aggregation number.[66] Much more material is seen to settle at a concentration of 150 mg/L. Consequently, it is reasonable to call the CNAC ~ 150 mg/L for this GOM asphaltene while noting that the CNAC represents a range of concentrations as expected for small aggregation numbers. Critical concentrations for nanoaggregate formation were obtained with high-Q ultrasonics, AC conductivity, DC conductivity, NMR hydrogen index, and NMR diffusion constants.[1,2] We also note that, in these centrifugation experiments, there was always some mass that accumulated at the outermost point on the wall even at small concentrations.[65] The quantity was difficult to determine for small concentrations. One expects that asphaltenes close to the far wall of the centrifuge tube should be collected. In addition, there might be a small inorganic component associated with clays that becomes collected.

Figure 14 shows the same value of CNAC for a different asphaltene compared to Figure 13. Moreover, the CNAC of the Latin American crude oil asphaltene (LAM) exhibits no detectable temperature dependence,[65] in reasonable agreement with a previous NMR study addressing the temperature dependence of the asphaltene CNAC.[21] The solubility product K of the nanoaggregate can be expressed in the form $K \sim \exp\{-\Delta G/kT\}$.

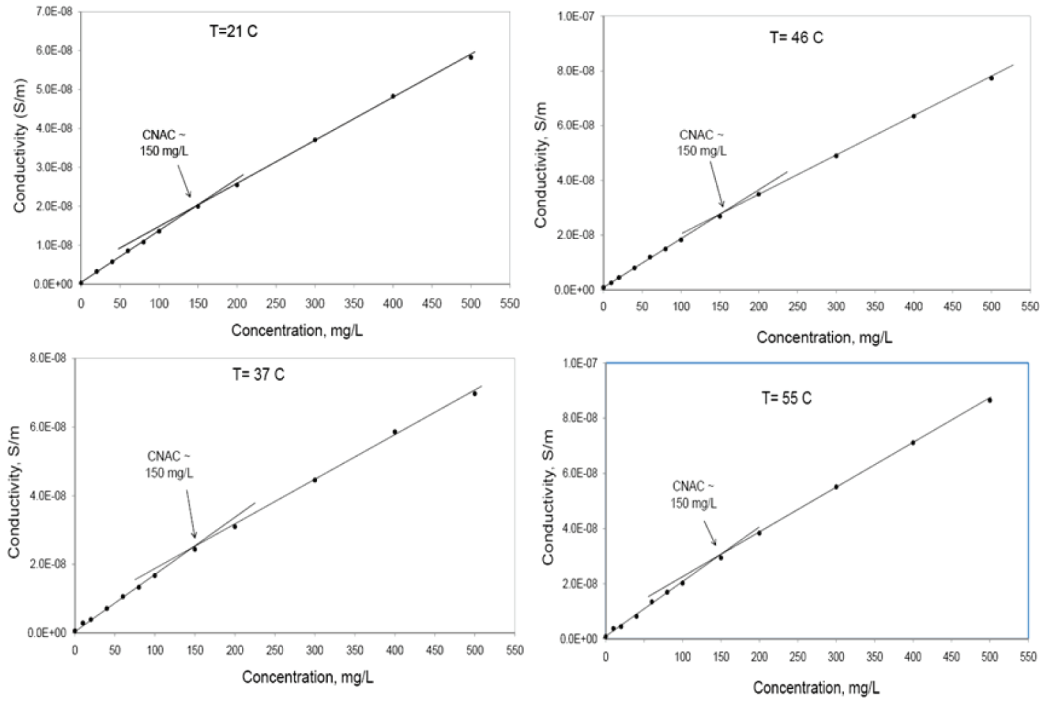

Figure 14. CNAC of LAM asphaltene is shown to be 150 mg/L. There is no detectable temperature dependence of the CNAC over a limited temperature range.[65]

dx.doi.org/10.1021/ef300185p | *Energy Fuels* 2012, 26, 3986−4003

$\Delta G = \Delta H - T\Delta S$. where ΔG, ΔH, and ΔS refer to the change of Gibbs free energy, enthalpy, and entropy of aggregate formation. The lack of temperature dependence of the CNAC indicates that nanoaggregate formation is primarily entropically driven (while of course the most favorable enthalpy configuration is favored). In aqueous systems, entropically driven micelle formation is common, essentially occurring because of the decreased excluded volume of the solvent. That is, the increase in solvent entropy upon aggregate formation is more important than the reduction of asphaltene entropy.

As repeatedly discussed,[1,2] asphaltene nanoaggregates have limited aggregation numbers because of molecular architecture. The attractive PAH is in the molecular interior, while the peripheral alkanes produce steric repulsion. Consequently, only a few (<10) molecules can aggregate before only repulsive alkanes are exposed to the outside. Nevertheless, with entropic formation, there can be aggregate number limits established as well. Extra large aggregates might have too low of an entropy, favoring an optimal aggregate size. This could be an important consideration for cluster formation, in that cluster size does not have molecular architecture limitations.

Critical Cluster Concentration (CCC). Perhaps the clearest demonstration of the asphaltene CCC is obtained by determining the kinetics of flocculation for asphaltene/toluene solutions subject to *n*-heptane addition, as shown in Figure 15.[67,68]

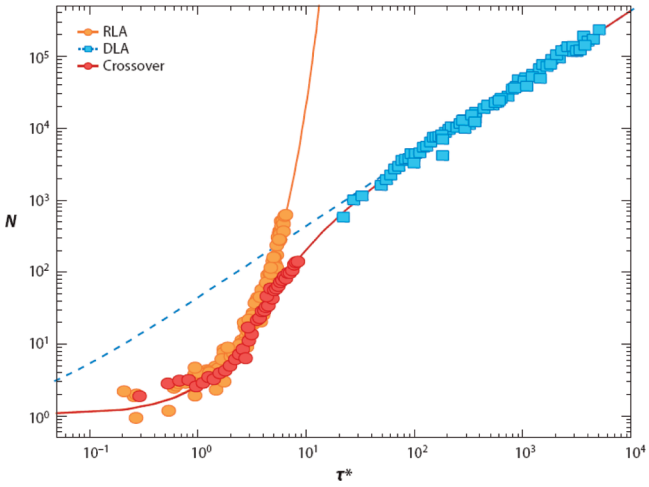

Figure 15. Aggregation number N as a function of the scaled time τ^*. Flocculation data for *n*-heptane addition to different asphaltene/toluene solutions. Orange circles represent data for 10 g/L asphaltene/toluene solution exhibiting reaction-limited aggregation (RLA). Blue squares represent data for a 1 g/L asphaltene/toluene solution exhibiting diffusion-limited aggregation (DLA). Red circles represent data for 5 g/L asphaltene/toluene solution exhibiting crossover aggregation kinetics.[68]

This figure clarifies that the concentration of cluster formation is more than 10 times greater than the concentration of nanoaggregate formation. Clusters are distinct from nanoaggregates.

For asphaltene/toluene solutions below CCC, *n*-heptane addition yields diffusion-limited aggregation. Upon destabilization with *n*-heptane addition, the nanoaggregates stick to each other upon collision. For *n*-heptane addition to asphaltene/toluene solutions above CCC, the clusters do not stick upon collision. A morphological change is needed on the surface of the fractal clusters to allow them to stick. This requirement of morphological change yields reaction-limited aggregation.[69] The CCC of asphaltenes was shown to be 2−5 g/L.

This informative flocculation study does not establish the size of clusters. For many reasons, this is an important parameter to determine. For the size determination of clusters, there is confluence of evidence from DC conductivity, SAXS and SANS results, and observation of asphaltene gradients in heavy oil reservoirs.

DC conductivity also gives a similar CCC for asphaltenes, as shown in Figure 16. In addition, the effect of the C5-insoluble

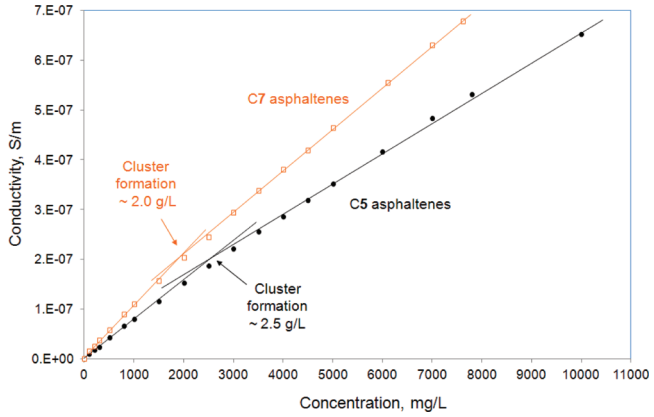

Figure 16. DC conductivity exhibits the critical clustering concentration of asphaltenes. For *n*-heptane asphaltenes, the CCC is 2.0 g/L.[65] By inclusion of the C5-insolubles and C7-solubles, the CCC changes but primarily trivially because of the dilution of C7-insolubles.

and C7-soluble fraction changed the CCC but primarily by a trivial dilution effect (C5-insolubles flocculate with the addition of *n*-pentane, and C7-insolubles flocculate with the addition of *n*-heptane). The same trivial dilution effect applies to the CNAC.[65] As with the CNAC, the change of Stokes drag at the CCC is not large, indicating that the cluster is not that much bigger than the nanoaggregate.

Size of the Asphaltene Nanoaggregate and Cluster. The size of the asphaltene nanoaggregate is obtained by AFM of corresponding Langmuir−Blodgett films (Figure 17). The films of asphaltene nanoaggregates are found to be ∼2 nm, whether grown from toluene or chloroform, which is in accordance with small aggregation numbers.[70,71]

The size of asphaltenes and clusters has been investigated by a series of studies specifically analyzing the absolute cross-section of SAXS and SANS together.[45,46] Figure 18 shows an example of this analysis.

More recently, the combined SAXS−SANS data interpretation indicated that the best fit to the data yielded a single PAH stack in the nanoaggregate, which is consistent with Figure 1, in terms of both the molecular structure and nanoaggregate structure. In addition, these data sets also show the existence of clusters.[46,72,73] A representation of the combined results is given in Figure 19.

Scattering data can be interpreted in various ways. To provide tight constraints for interpretation in Figure 19, the scattering data have been acquired (1) on an absolute intensity scale, (2) on a large scattering vector (length scale) domain, (3) using different scattering probes (X-ray and neutrons), and (4) in deuterated and hydrogenated toluene mixtures to vary the scattering length density of the solvent.[46] In this manner, the

dx.doi.org/10.1021/ef300185p | Energy Fuels 2012, 26, 3986−4003

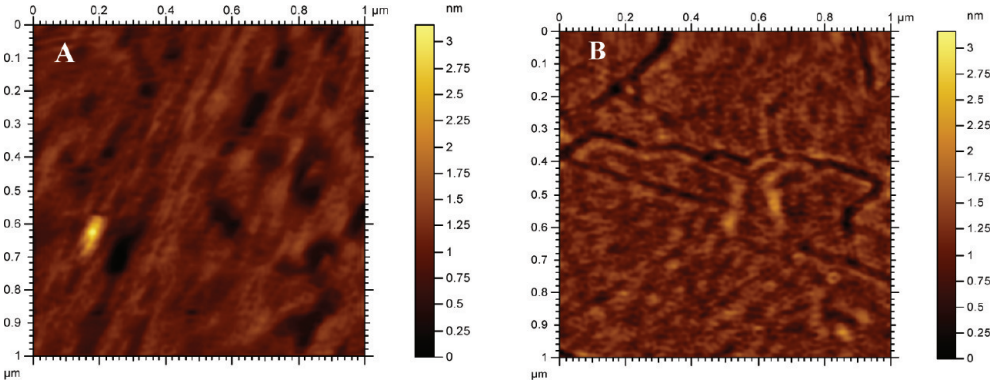

Figure 17. AFM of a Langmuir–Blodgett film of asphaltene nanoaggregates on highly oriented pyrolytic graphite (A) deposited from toluene[70] or (B) deposited from chloroform.[71] The nanoaggregate layer is approximately 2 nm thick.

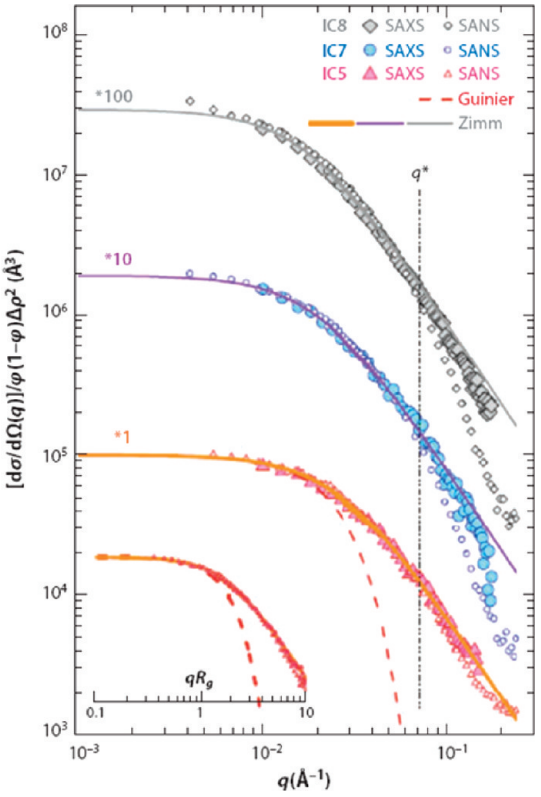

Figure 18. Comparison between SAXS (solid points) and SANS (hollow points) spectra. Variations of the normalized cross-section $I(q)/\varphi\Delta\rho^2$ as a function of the wave-scattering vector q for solutions of different asphaltenes in toluene. The dotted and solid lines represent the Guinier and Zimm approximations, respectively, in the small-q domain. The contrast between SAXS sensitivity to electron density and, thus, the PAH stack versus the SANS sensitivity to hydrogen and, thus, the peripheral alkanes gives the length scale of the interior PAH stack of the nanoaggregate, approximately 1.4 nm.[45]

model coming from fitting the scattering data is highly selective if not unique, and strong conclusions can be obtained. Polydispersity is included of course and can alter the parameter magnitude to a degree. Nevertheless, the clear conclusion is the existence of two colloidal structures and not just one.[46]

Figure 19 shares many similarities with the Yen–Mullins model of Figure 1, for example, the island architecture with a somewhat large PAH. Not one but two distinct nanocolloidal species are obtained. The smaller species is a nanoaggregate of small aggregation number with an aromatic core and an alkane shell. A cluster with a small aggregation number of nanoaggregates is obtained. While the overall length scales for the nanospecies in Figures 1 and 19 are similar, there are specific differences. For example, the sizes of the asphaltene PAH are similar but not identical. In addition, proposed molecular structures must explicitly account for the energetics of ring systems, as discussed.[10,74] In our view, these differences are secondary to the overall similarities. Future studies will shed light on these issues. It is also important to remember that there are multiple types of sizes that appear in these different studies. For example, the SANS and SAXS studies are sensitive to the radius of gyration of the species in question (as well as its actual geometry). The DC conductivity studies and asphaltene molecular diffusion studies are sensitive to the hydrodynamic radius, while the centrifugation studies and the oilfield studies are sensitive to the effective physical radius. Thus, even for the exact same species, different studies will obtain somewhat different effective sizes.

A question arises as to why the cluster size is limited. If cluster formation is enthalpically driven, it is hard to understand why aggregation would cease at this nano length scale. However, if cluster formation is entropically driven as nanoaggregate formation is, then it makes sense that there is an optimal size. Too little aggregation, and the solvent entropy is too low. Too much aggregation, and the asphaltene entropy is too low. Indeed, studies on related inverse micelles support the idea of an entropy drive for the formation of nanoparticles.[75] Nevertheless, the cluster size would then depend much more upon environmental conditions than the nanoaggregate because of the molecular geometry constraint on the nanoaggregate size. Indeed, this is just what was observed in the SANS and SAXS studies.[72,73]

Recent work has shown that phase behavior properties of asphaltenes in crude oils in the presence of various solvents is best accounted for with the presumption of the existence of asphaltene nanoaggregates in the crude oil.[76] Specifically, Wiehe plots can be prepared for crude oils, where asphaltene precipitation onset is plotted against the addition of *n*-heptane and Heptol mixtures to the crude oil. The observed characteristics of the Wiehe phase behavior plots can be obtained via a regular solution approach presuming asphaltene nanoaggregates.[76] A regular solution theory, such as the Flory–Huggins theory, has been used successfully to treat many aspects of asphaltene phase behavior.[77,78]

dx.doi.org/10.1021/ef300185p | *Energy Fuels* 2012, 26, 3986–4003

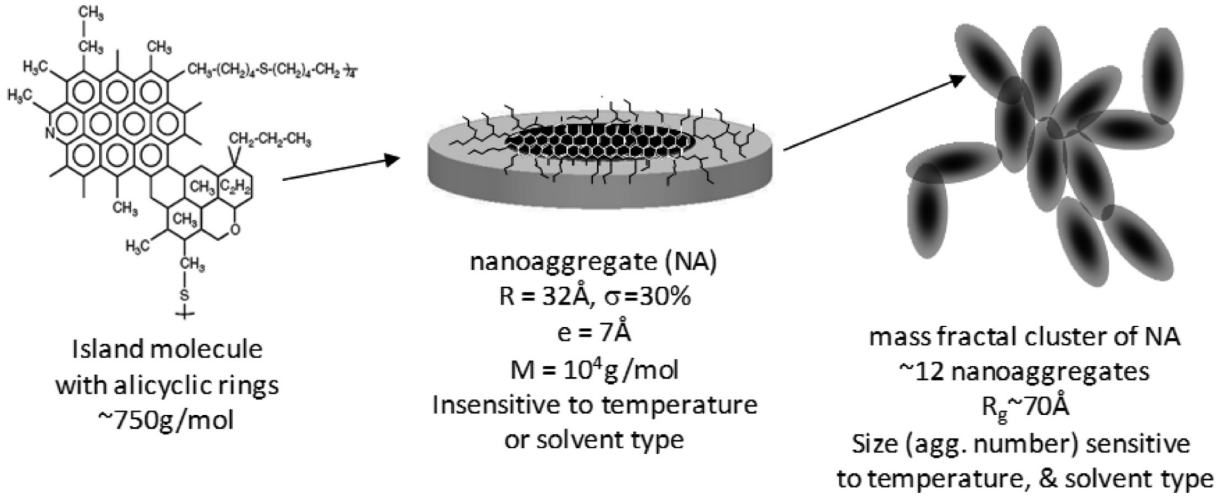

Figure 19. Asphaltene nanoscience model most consistent with combined SANS and SAXS studies.[46,72,73] This model is very consistent with the Yen–Mullins model of Figure 1 and is very encouraging that major features of asphaltene nanoscience are being resolved.

FIRST PREDICTIVE EQUATION OF STATE FOR ASPHALTENE GRADIENTS IN OILFIELD RESERVOIRS

The implications of resolving asphaltene nanoscience are dramatic. With the resolution of the size of asphaltene molecules and nanocolloidal species, the gravity term can now be determined in an equation of state. The gravity term has been aded to the Flory–Huggins equation that has been used extensively in treating asphaltene phase behavior.[77,78] We refer to this new equation as the FHZ EoS for Dr. Julian Y. Zuo, who is leading the effort to use this new thermodynamic model to address a variety of major oilfield concerns.[79−81] The FHZ EoS is given below[79−81]

$$\frac{\mathrm{OD}(h_2)}{\mathrm{OD}(h_1)} = \frac{\phi_a(h_2)}{\phi_a(h_1)} = \exp\left(\frac{v_a g \Delta\rho (h_2 - h_1)}{RT} + \left(\frac{v_a}{v}\right)_{h_2} - \left(\frac{v_a}{v}\right)_{h_1} - \frac{v_a[(\delta_a - \delta)_{h_2}{}^2 - (\delta_a - \delta)_{h_1}{}^2]}{RT}\right) \quad (1)$$

where $\mathrm{OD}(h_i)$ is the optical density as a result of electronic absorption (cf. Figure 9) at height h_i in the reservoir, $\phi_a(h_i)$ is the asphaltene content at height h_i, v_a is the molar volume of the particular asphaltene species (cf. Figure 1), g is earth's gravitational acceleration, R is the ideal gas constant, T is the temperature, v is the molar volume of the liquid-phase crude oil, and δ_a and δ are the solubility parameters of asphaltene and the crude oil, respectively. For condensates, the relevant asphaltene volume is the molecule. For black oils, the relevant asphaltene volume is the nanoaggregate. For mobile heavy oil, the relevant asphaltene volume is the cluster. Mobile heavy oils have viscosities up to roughly one thousand cP and can be produced conventionally.

To employ the FHZ EoS, one can use standard laboratory determinations of parameters, such as the asphaltene solubility parameter. The crude oil solubility parameter for a live crude oil (with its reservoir solution gas) depends upon the GOR of the crude oil.[79−81] Indeed, the FHZ EoS is compatible with measurements performed downhole in oil wells (downhole fluid analysis) during sample acquisition of crude oils,[82] thereby making the FHZ EoS very important from a practical standpoint. The asphaltene solubility parameter can be estimated without much difficulty, and for evaluating asphaltene gradients in reservoirs, a single parameter value suffices, (e.g., 21.85 $\mathrm{MPa}^{1/2}$ at 298 K).[81]

OILFIELD CASE STUDIES

Asphaltene Gradients in Reservoir Crude Oils. Many recent oilfield studies have shown the utility of this combination of asphaltene nanoscience and the FHZ EoS. Figure 20 shows the application of this equation of state for each of the three asphaltene species in Figure 1 for three different reservoirs.[83]

In all three cases, the asphaltenes in the reservoir crude oils were shown to obey the FHZ EoS; thus, the asphaltenes are equilibrated. In all three cases, the reservoirs were shown to be in flow communication by production, which is consistent with an equilibrated fluid column.[84] For the low GOR black oil (middle in Figure 20), the asphaltene gradient is dominated by the gravitation term of eq 1. For the mobile heavy oil (right in Figure 20), again, the asphaltene gradient is dominated by the gravity term. Most importantly, the two gradients differ by a factor of 50. That is, there is an asphaltene concentration difference of a factor of 2 in 1000 m of oil column height for the nanoaggregates (black oil), while for clusters (heavy oil), there is an asphaltene concentration difference of a factor of 2 in 20 m. Recent data on heavy oilfields from the Gulf of Mexico, Russia, Saudi Arabia, and Ecuador all exhibit the same gradients because of asphaltene clusters.[85] This difference in asphaltene gradient between nanoaggregates and clusters occurs because the factor of 2.5 difference between them in linear dimension becomes cubed in the asphaltene volume term v_a and is than placed in the argument of the exponential of the Boltzmann distribution, (cf. eq 1; $\exp\{-v_a g \Delta\rho h/kT\}$). Because viscosity of heavy oil exponentially depends upon the asphaltene content and the oil flow rate inversely depends upon viscosity, the asphaltene gradients are very important. For example, the asphaltene gradient on the right in Figure 20 corresponds to 6 cP at the top of the column and 200 cP at 20 m lower. This has huge implications in heavy oilfields around the world.[85]

Reservoir Connectivity. Most importantly, the Yen–Mullins model applies to not only asphaltenes in toluene but also asphaltenes in reservoir crude oils. This auspicious circumstance bodes well for many important field applications. Because asphaltene equilibration is a slow process on a geologic time scale, the implication is that these reservoirs with equilibrated asphaltenes are connected

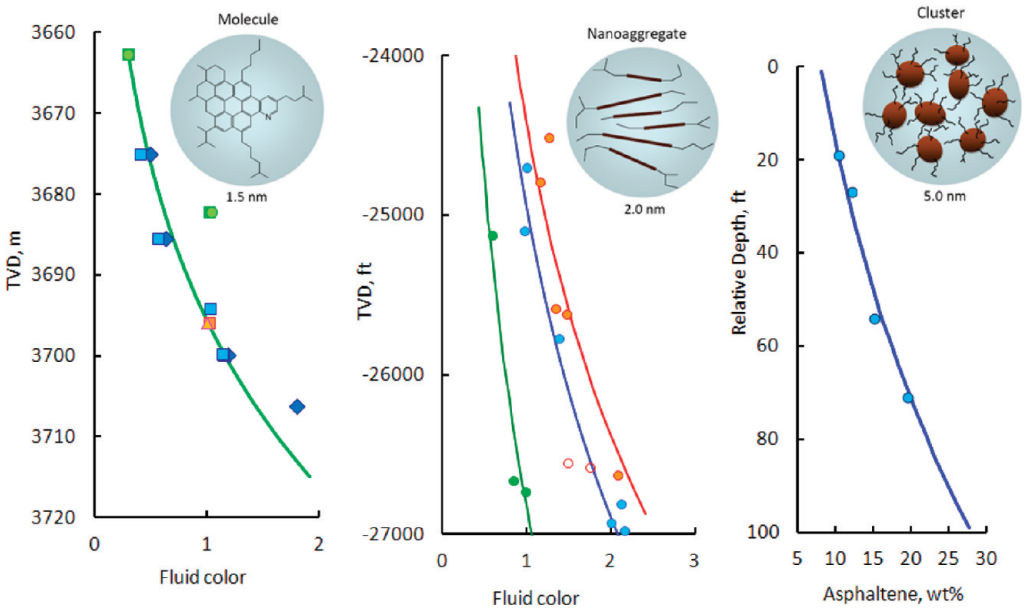

Figure 20. Asphaltene gradients in three different oilfield reservoirs are shown. (Left) Condensate with a true molecular solution of asphaltene (or asphaltene-like) molecules, (Middle) Low GOR black oil with asphaltene nanoaggregates. (Right) Mobile heavy oil with asphaltene clusters. Note that the larger clusters produce a gravitational gradient 50× larger than the low GOR black oil. For the condensate, the GOR gradient helps create the asphaltene gradient.[83]

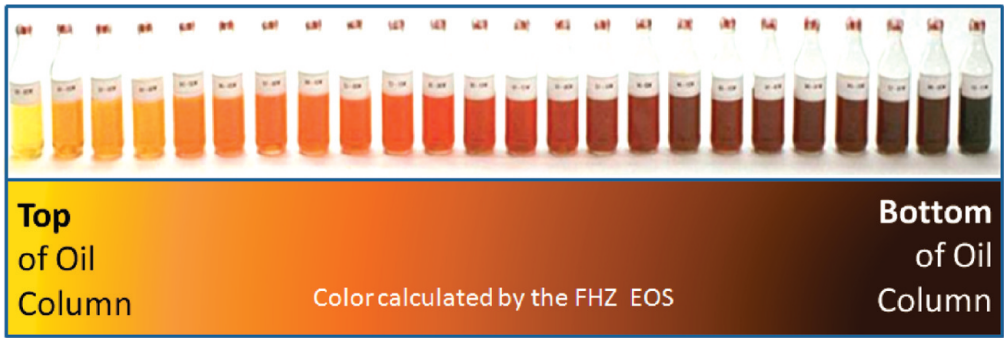

Figure 21. FHZ EoS can fit the famous series of crude oils from a single oil column deepwater, Gulf of Mexico (courtesy of Hani Elshahawi, Shell Exploration and Production Company). These are dead crude oils. The solution gas has been removed. One visually sees a giant asphaltene gradient that is reproduced by the FHZ EoS (using nanoaggregates).[83]

without flow barriers.[84] In all three cases in Figure 20, oil production proved this to be true.[83] We also note that recent field studies suggest that the size of clusters shows some variability from one oilfield to another. This observation, if validated, is consistent with the SAXS and SANS studies[72,73] regarding somewhat variable cluster size and is a current area of research.

Disequilibrium. Another major success of the FHZ EoS is the ability to account for the gigantic asphaltene gradient in a single oil column deepwater, Gulf of Mexico. Figure 21 shows the asphaltene gradient, which is obvious to the eye, along with the results of the FHZ EoS analysis.[83] This gradient was created by a late gas charge into the reservoir. The gas quickly migrates to the top of the reservoir and then diffuses down. Where the solution gas is high at the top of the oil column, the asphaltenes are expelled. Toward the base of the oil column, the solution gas remains low because the gas has not had sufficient time to reach the base by diffusion. Low solution gas is compatible with high asphaltene content. This variable solution gas is grossly out of equilibrium. The asphaltenes locally equilibrate according to the solution gas content in the oil, but the asphaltene content is also grossly out of equilibrium when considering the column as a whole.[83]

Tar Mat Formation. In similar oilfields with a later gas charge but where the solution gas has increased (diffused) all of the way to the bottom of the oil column, the asphaltene can be expelled in bulk, creating a tar mat at the base of the column.[86] Figure 22 shows a thin section from the core, showing the asphaltene-rich tar mat.[86] Tar mats have not been well-understood in the oil industry, the FHZ EoS coupled with the Yen–Mullins model is providing substantial guidance for this issue. Perturbed-chain statistical associating fluid theory (PC-SAFT) modeling has recently been employed to model asphaltene gradients and also offers a promising approach.[87] PC-SAFT modeling has been successful in modeling asphaltene phase behavior.[88] Nevertheless, to obtain a 50× larger gradient for mobile heavy oil than for low GOR black oil, it is likely that PC-SAFT modeling will need to explicitly incorporate the Yen–Mullins model.

Kinetics. Transport of asphaltenes through porous media is dependent upon the existence of multiple colloidally stable species. That is, destabilization of nanoaggregates can produce asphaltene clusters that then create high concentrations of asphaltene toward the case of the oil column (cf. right in Figure 20). It is at the base of the column where the highest

dx.doi.org/10.1021/ef300185p | Energy Fuels 2012, 26, 3986–4003

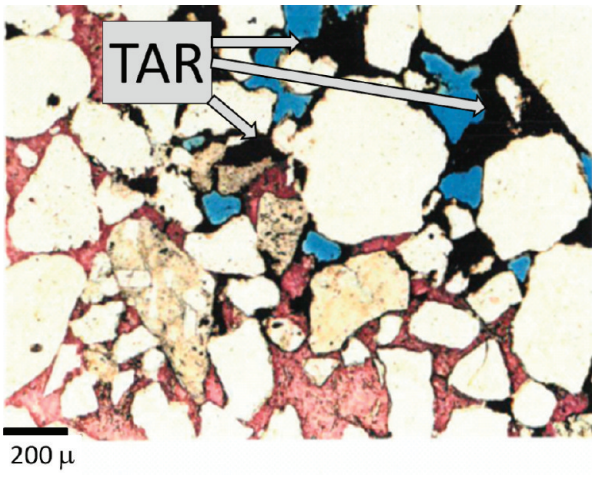

Figure 22. Tar that formed at the base of a high GOR oil column. This asphaltene-rich tar formed on a cemented sandstone and, thus, not at an oil–water contact (water had nothing to do with this tar mat formation). Gas diffusion into the oil destabilized the asphaltene, causing phase instability at the base of the column.[86]

asphaltene concentrations are found that can exceed the solvency of the crude oil for asphaltenes, thereby inducing phase instability there. Nevertheless, it is important to realize that processes on geologic time are slow and can involve additional complexities. Figure 23 shows that asphaltene flocculation times can become quite long when the destabilization of asphaltenes is slight.[89]

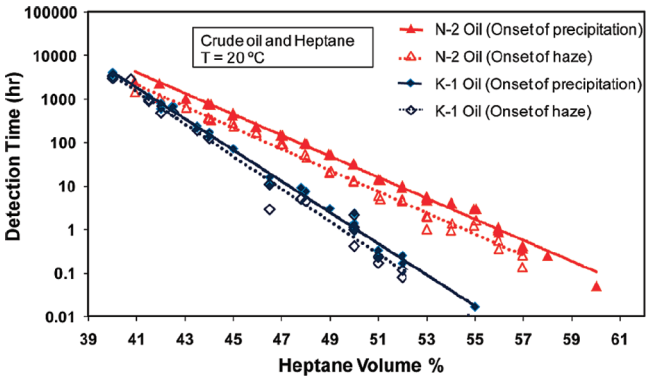

Figure 23. Detection times for the onset of precipitation and onset of haze for varying heptane concentrations using K-1 and N-2 crude oils.[89]

These slow kinetics are accompanied by small particle size, especially early in the flocculation process.[90] It is plausible that these slow kinetics and small flocs play a role in the migration of asphaltenes through reservoirs. The Stokes velocity of an asphaltene cluster is exceedingly small. There might be a role for very small flocs, for example, 10 nm in size, in this migration process and is an area of current research. Nevertheless, measured gradients in mobile heavy oils are consistent with cluster size (5 nm).[85] Any explanation regarding asphaltene transport through reservoirs must be consistent with this observation.

CONCLUSION

The Yen–Mullins model, also known as the modified Yen model, addresses the molecular and nanocolloidal species of asphaltenes in laboratory solvents and reservoir crude oils. After the first publication of this model, many studies have been published using a wide variety of methods supporting all major components of the Yen–Mullins model. In particular, unimolecular decomposition studies obtain strong evidence for the "island" molecular architecture, with a single PAH in the molecular core. A bulk decomposition study proved that island model compounds can be converted to archipelago compounds, helping to explain discrepancies associated with bulk decomposition studies. A new NMR study finally put ^{13}C NMR studies in alignment with many other techniques regarding the number of fused rings in asphaltene PAHs. An unusual study identified the origin of the blue color of a light crude oil as being due to fluorescence from perylene, a five fused ring PAH. This observation supports conclusions about the sizes of PAHs that occur in asphaltenes. Optical interrogation along with MO calculations of the asphaltene PAH distribution has been extended to the triplet-state manifold with continuing consistency. Approximately seven fused ring PAHs represent the asphaltene population centroid. Centrifugation and DC conductivity studies reinforce reported aggregation concentrations of nanoaggregates and clusters. The existence and size of these nanocolloidal species are strongly reinforced by combined SANS and SAXS studies. The Yen–Mullins model has enabled development of the industry's first equation of state for asphaltene gradients, the FHZ EoS. In turn, this has been exploited in conjunction with new chemical analysis methods in the oilfield to characterize asphaltene gradients and instability in various reservoir crude oil from condensates to mobile heavy oils. The tremendous utility of this approach is becoming evident in numerous oilfield case studies. Kinetic studies in both the laboratory and the oilfield are creating a link to explore reservoir concerns. The field of asphaltene science is rapidly evolving, and the corresponding technology applications are rapidly expanding. The vision of petroleomics is being realized in the laboratory and the reservoir. The proper chemical understanding of the "third" enigmatic phase, the solid asphaltenes, of crude oil, coupled with the traditional understanding of gas and liquid phases, is dramatically improving petroleum science, with auspicious implications for evaluation and exploitation of oilfield reservoirs.

AUTHOR INFORMATION

Corresponding Author

*E-mail: mullins1@slb.com.

Notes

The authors declare no competing financial interest.

REFERENCES

(1) Mullins, O. C. The modified Yen model. *Energy Fuels* **2010**, *24*, 2179–2207.

(2) Mullins, O. C. The asphaltenes. *Annu. Rev. Anal. Chem.* **2011**, *4*, 393–418.

(3) *Chemistry of Asphaltenes*; Bunger, J. W., Li, N. C., Eds.; American Chemical Society: Washington, D.C., 1981.

(4) *Bitumens, Asphalts and Tar Sands*; Chilingarian, G. V., Yen, T. F., Eds.; Elsevier Scientific Publishing Co.: Amsterdam, The Netherlands, 1978.

(5) *Asphaltenes and Asphalts*; Chilingarian, G. V., Yen, T. F., Eds.; Elsevier Scientific Publishing Co.: Amsterdam, The Netherlands, 1994; Vol. *1*.

(6) *Asphaltenes and Asphalts*; Yen, T. F., Chilingarian, G. V., Eds.; Elsevier Scientific Publishing Co.: Amsterdam, The Netherlands, 2000; Vol. *2*.

(7) *Asphaltenes, Fundamentals and Applications*; Sheu, E. Y., Mullins, O. C., Eds.; Plenum Press: New York, 1995.

(8) *Structures and Dynamics of Asphaltenes*; Mullins, O. C., Sheu, E. Y., Eds.; Plenum Press: New York, 1998.

(9) *Asphaltenes, Heavy Oils and Petroleomics*; Mullins, O. C., Sheu, E. Y., Hammami, A., Marshall, A. G., Eds.; Springer: New York, 2007.
(10) Ruiz-Morales, Y. Aromaticity in pericondensed cyclopenta-fused polycyclic aromatic hydrocarbons determined by density functional theory nucleus-independent chemical shifts and the Y-rule—Implications in oil asphaltene stability. *Can. J. Chem.* **2009**, *87*, 1280−1295.
(11) Sabbah, H.; Morrow, A. L.; Pomerantz, A. E.; Zare, R. N. Evidence for island structures as the dominant architecture of asphaltenes. *Energy Fuels* **2011**, *25*, 1597−1604.
(12) Boduszynski, M. M. In *Chemistry of Asphaltenes*; Bunger, J. W., Li, N. C., Eds.; American Chemical Society (ACS): Washington, D.C., 1981; Chapter 7.
(13) Rodgers, R. P.; Marshall, A. G. Petroleomics: Advanced characterization of petroleum derived materials by Fourier transform ion cyclotron resonance mass spectrometry (FT-ICR MS). In *Asphaltenes, Heavy Oils and Petroleomics*; Mullins, O. C., Sheu, E. Y., Hammami, A., Marshall, A. G., Eds.; Springer: New York, 2007; Chapter 3.
(14) Hortal, A. R.; Hurtado, P. M.; Martınez-Haya, B.; Mullins, O. C. Molecular weight distributions of coal and petroleum asphaltenes from laser desorption ionization experiments. *Energy Fuels* **2007**, *21*, 2863−2868.
(15) Qian, K.; Edwards, K. E.; Siskin, M.; Olmstead, W. N.; Mennito, A. S.; Dechert, G. J.; Hoosain, N. E. Desorption and ionization of heavy petroleum molecules and measurement of molecular weight distributions. *Energy Fuels* **2007**, *21*, 1042−1047.
(16) Pinkston, D. S.; Duan, P.; Gallardo, V. A.; Habicht, S. C.; Tan, X.; Qian, K.; Gray, M.; Muellen, K.; Kenttamaa, H. Analysis of asphaltenes and asphaltene model compounds by laser-induced acoustic desorption/Fourier transform ion cyclotron resonance mass spectrometry. *Energy Fuels* **2009**, *23*, 5564−5570.
(17) Groenzin, H.; Mullins, O. C. Asphaltene molecular size and structure. *J. Phys. Chem. A* **1999**, *103*, 11237−11245.
(18) Groenzin, H.; Mullins, O. C. Molecular sizes of asphaltenes from different origin. *Energy Fuels* **2000**, *14*, 677.
(19) Wargadalam, V. J.; Norinaga, K.; Iino, M. Size and shape of a coal asphaltene studied by viscosity and diffusion coefficient measurements. *Fuel* **2002**, *81*, 1403−1407.
(20) Andrews, A. B.; Guerra, R.; Mullins, O. C.; Sen, P. N. Diffusivity of asphaltene molecules by fluorescence correlation spectroscopy. *J. Phys. Chem. A* **2006**, *110*, 8095.
(21) Freed, D. E.; Lisitza, N. V.; Sen, P. N.; Song, Y. Q. A study of asphaltene nanoaggregation by NMR. *Energy Fuels* **2009**, *23*, 1189−1193.
(22) Zajac, G. W.; Sethi, N. K.; Joseph, J. T. Molecular imaging of asphaltenes by scanning tunneling microscopy: Verification of structure from ^{13}C and proton NMR data. *Scanning Microsc.* **1994**, *8*, 463.
(23) Sharma, A.; Groenzin, H.; Tomita, A.; Mullins, O. C. Probing order in asphaltenes and aromatic ring systems by HRTEM. *Energy Fuels* **2002**, *16*, 490.
(24) Ruiz-Morales, Y.; Wu, X.; Mullins, O. C. Electronic absorption edge of crude oils and asphaltenes analyzed by molecular orbital calculations with optical spectroscopy. *Energy Fuels* **2007**, *21*, 944.
(25) Ruiz-Morales, Y.; Mullins, O. C. Simulated and measured optical absorption spectra of asphaltenes. *Energy Fuels* **2009**, *23*, 1169−1177.
(26) Bouhadda, Y.; Bormann, D.; Sheu, E. Y.; Bendedouch, D.; Krallafa, A.; Daaou, M. Characterization of Algerian Hassi−Messaoud asphaltene structure using Raman spectrometry and X-ray diffraction. *Fuel* **2007**, *86*, 1855−1864.
(27) Bergmann, U.; Groenzin, H.; Mullins, O. C.; Glatzel, P.; Fetzer, J.; Cramer, S. P. Carbon K-edge X-ray Raman spectroscopy supports simple yet powerful description of aromatic hydrocarbons and asphaltenes. *Chem. Phys. Lett.* **2003**, *369*, 184.
(28) Sheremata, J. M.; Gray, M. R.; Dettman, H. D.; McCaffrey, W. C. Quantitative molecular representation and sequential optimization of Athabasca asphaltenes. *Energy Fuels* **2004**, *18*, 1377−1384.
(29) Buenrostro-Gonzalez, E.; Groenzin, H.; Lira-Galeana, C.; Mullins, O. C. The overriding chemical principles that define asphaltenes. *Energy Fuels* **2001**, *15*, 972.
(30) Badre, S.; Goncalves, C. C.; Norinaga, K.; Gustavson, G.; Mullins, O. C. Molecular size and weight of asphaltene and asphaltene solubility fractions from coals, crude oils and bitumen. *Fuel* **2006**, *85*, 1.
(31) McKenna, A. M.; Purcell, J. M.; Rodgers, R. P.; Marshall, A. G. *Proceedings of the Petrophase 10th International Conference on Petroleum Phase Behavior and Fouling*; Rio de Janeiro, Brazil, June 14−19, 2009.
(32) Rubinstein, I.; Spyckerelle, C.; Strausz, O. P. Pyrolysis of asphaltenes. *Geochim. Cosmochim. Acta* **1979**, *43*, 1−6.
(33) Goncalves, S.; Castillo, J.; Fernandez, A.; Hung, J. Absorbance and fluorescence spectroscopy on the aggregation of asphaltene toluene solutions. *Fuel* **2004**, *83*, 1823.
(34) Andreatta, G.; Bostrom, N.; Mullins, O. C. High-Q ultrasonic determination of the critical nanoaggregate concentration of asphaltenes and the critical micelle concentration of standard surfactants. *Langmuir* **2005**, *21*, 2728.
(35) Sheu, E. Y.; Long, Y.; Hamza, H.; Asphaltene self-association and precipitation in solvents—AC conductivity measurements. In *Asphaltene, Heavy Oils and Petroleomics*; Mullins, O. C., Sheu, E. Y., Hammami, A., Marshall, A. G., Eds.; Springer: New York, 2007; Chapter 10.
(36) Zeng, H.; Song, Y. Q.; Johnson, D. L.; Mullins, O. C. Critical nanoaggregate concentration of asphaltenes by low frequency conductivity. *Energy Fuels* **2009**, *23*, 1201−1208.
(37) Goual, L.; Abudu, A. Predicting the adsorption of asphaltenes from their electrical conductivity. *Energy Fuels* **2010**, *24*, 469−474.
(38) Indo, K.; Ratulowski, J.; Dindoruk, B.; Mullins, O. C. Asphaltene nanoaggregates measured in a live crude oil by centrifugation. *Energy Fuels* **2009**, *23*, 4460−4469.
(39) Mostowfi, F.; Indo, K.; Mullins, O. C.; McFarlane, R. Asphaltene nanoaggregates and the critical nanoaggregate concentration from centrifugation. *Energy Fuels* **2009**, *23*, 1194−1200.
(40) Yen, T. F.; Erdman, J. G.; Pollack, S. S. Investigation of the structure of petroleum asphaltenes by X-ray diffraction. *Anal. Chem.* **1961**, *33* (11), 1587−1594.
(41) Sheu, E. Y. Colloidal properties of asphaltenes in organic solvents. In *Asphaltenes—Fundamentals and Applications*; Sheu, E. Y., Mullins, O. C., Eds.; Plenum Press: New York, 1995; Chapter 1.
(42) Sheu, E. Y. Petroleomics and characterization of asphaltene aggregates using small angle scattering. In *Asphaltene, Heavy Oils and Petroleomics*; Mullins, O. C., Sheu, E. Y., Hammami, A., Marshall, A. G., Eds.; Springer: New York, 2007; Chapter 14.
(43) Wiehe, I. A.; Liang, K. S. Asphaltenes, resins, and other petroleum macromolecules. *Fluid Phase Equilib.* **1996**, *117*, 201−210.
(44) Barré, L.; Simon, S.; Palermo, T. Solution properties of asphaltenes. *Langmuir* **2008**, *24* (8), 3709−3717.
(45) Barré, L.; Jestin, J.; Morisset, A.; Palermo, T.; Simon, S. Relation between nanoscale structure of asphaltene aggregates and their macroscopic solution properties. *Oil Gas Sci. Technol.* **2009**, *64*, 617−628.
(46) Eyssautier, J.; Levitz, P.; Espinat, D.; Jestin, J.; Gummel, J.; Grillo, I.; Barré, L. Insight into asphaltene nanoaggregate structure inferred by small angle neutron and X-ray scattering. *J. Phys. Chem. B* **2011**, *115*, 6827−6837.
(47) Mullins, O. C.; Betancourt, S. S.; Cribbs, M. E.; Creek, J. L.; Andrews, B. A.; Dubost, F.; Venkataramanan, L. The colloidal structure of crude oil and the structure of reservoirs. *Energy Fuels* **2007**, *21*, 2785−2794.
(48) Sabbah, H.; Pomerantz, A. E.; Wagner, M.; Mullen, K.; Zare, R. N. Laser desorption single-photon ionization of asphaltenes: mass range, compound sensitivity, and matrix effects. *Energy Fuels*, in press.
(49) Pomerantz, A. E.; Hammond, M. R.; Morrow, A. L.; Mullins, O. C.; Zare, R. N. Two step laser mass spectrometry of asphaltenes. *J. Am. Chem. Soc.* **2008**, *130* (23), 7216−7217.
(50) Pomerantz, A. E.; Hammond, M. R.; Morrow, A. L.; Mullins, O. C.; Zare, R. N. Asphaltene molecular weight distribution determined

by two-step laser mass spectrometry. *Energy Fuels* **2009**, *23*, 1162−1168.
(51) Curiale, J.; Frolov, E. B. Occurrence and origin of olefins in crude oil. A critical review. *Org. Geochem.* **1998**, *29*, 397−408.
(52) Saxby, J. D.; Bennet, A. J. R.; Corcoran, J. F.; Lambert, D. E.; Riley, K. W. Petroleum generation: Simulation over six years of hydrocarbon formation from torbanite and brown coal in subsiding basin. *Org. Geochem.* **1986**, *9*, 69−81.
(53) Alshareef, A. H.; Scherer, A.; Tan, X.; Azyat, K.; Stryker, J. M.; Tywinski, R. R.; Gray, M. R. Formation of archipelago structures during thermal cracking implicates a chemical mechanism for the formation of petroleum asphaltenes. *Energy Fuels* **2011**, *25*, 2130−2136.
(54) Borton, D.; Pinkston, D. S.; Hurt, M. R.; Tan, X.; Azyat, K.; Tywinsky, R.; Gray, M.; Qian, K.; Kenttamaa, H. I. Molecular structures of asphaltenes based on the dissociation reactions of their ions in mass spectrometry. *Energy Fuels* **2010**, *24* (10), 5548−5559.
(55) Borton, D.; Pinkston, D. S.; Gray, M. R.; Kenttamaa, H. A comparison of model compounds and asphaltenes, island vs. archipelago models. *Proceedings of the Petrophase 12th International Conference on Petroleum Phase Behavior and Fouling*; London, U.K., July 10−14, 2011.
(56) Juyal, P.; McKenna, A. M.; Yen, A.; Rodgers, R. P.; Reddy, C. M.; Nelson, R. K.; Andrews, A. B.; Atolia, E.; Allenson, S. J.; Mullins, O. C.; Marshall, A. G. Analysis and identification of biomarkers and origin of blue color in an unusually blue crude oil. *Energy Fuels* **2011**, *25*, 172−182.
(57) Klee, T.; Masterson, T.; Miller, B.; Barrasso, E.; Bell, J.; Lepkowicz, R.; West, J.; Haley, J. E.; Schmitt, D. L.; Flikkema, J. L.; Cooper, T. M.; Ruiz-Morales, Y.; Mullins, O. C. Triplet electronic spin-states of crude oils and asphaltenes. *Energy Fuels* **2011**, *25*, 2065−2075.
(58) Scotti, R.; Montanari, L. Molecular structure and intermolecular interaction of asphaltenes by FTIR, NMR and EPR. In *Structures and Dynamics of Asphaltenes*; Mullins, O. C., Sheu, E. Y., Eds.; Plenum Press: New York, 2005; pp 79−114.
(59) Andrews, A. B.; Edwards, J. C.; Mullins, O. C.; Pomerantz, A. E. A comparison of coal and petroleum asphaltenes by ^{13}C nuclear magnetic resonance and DEPT. *Energy Fuels* **2011**, *25*, 3068−3076.
(60) Andrews, A. B.; Shih, W.-C.; Mullins, O. C.; Norinaga, K. Molecular size of various asphaltenes by fluorescence correlation spectroscopy. *Appl. Spectrosc.* **2011**, *65*, 1348−1356.
(61) Durand, E.; Clemancey, M.; Lancelin, J.-M.; Verstraete, J.; Espinat, D.; Quoineaud, A.-A. Effect of chemical composition on asphaltenes aggregation. *Energy Fuels* **2010**, *24*, 1051−1062.
(62) Siskin, M.; Kelemen, S. R.; Eppig, C. P.; Brown, L. D.; Afeworki, M. Asphaltene molecular structure and chemical influences on the morphology of coke produced in delayed coking. *Energy Fuels* **2006**, *20*, 1227−1234.
(63) Buch, L.; Groenzin, H.; Buenrostro-Gonzalez, E.; Andersen, S. I.; Lira-Galeana, C.; Mullins, O. C. Effect of hydrotreatment on asphaltene fractions. *Fuel* **2003**, *82*, 1075.
(64) Goual, L. Impedance spectroscopy of petroleum fluids at low frequency. *Energy Fuels* **2009**, *23*, 2090−2094.
(65) Goual, L.; Sedghi, M.; Zeng, H.; Mostowfi, F.; McFarlane, R.; Mullins, O. C. On the formation and properties of asphaltene nanoaggregates and cluster by DC-conductivity and centrifugation. *Fuel* **2011**, *90*, 2480−2490.
(66) Friberg, S. E. Micellization. In *Asphaltenes, Heavy Oils and Petroleomics*; Mullins, O. C., Sheu, E. Y., Hammami, A., Marshall, A. G., Eds.; Springer: New York, 2007; Chapter 7.
(67) Anisimov, M. A.; Yudin, I. K.; Nikitin, V.; Nikolaenko, G.; Chernoutsan, A.; Toulhoat, H.; Frot, D.; Briolant, Y. Asphaltene aggregation in hydrocarbon solutions studied by photon correlation spectroscopy. *J. Phys. Chem.* **1995**, *99* (23), 9576−9580.
(68) Yudin, I. K.; Anisimov, M. A. Dynamic light scattering monitoring of asphaltene aggregation in crude oils and hydrocarbon solutions. In *Asphaltenes, Heavy Oils and Petroleomics*; Mullins, O. C., Sheu, E. Y., Hammami, A., Marshall, A. G., Eds.; Springer: New York, 2007; Chapter 17.
(69) Mullins, W. W. Private communication. Carnegie-Mellon University: Pittsburgh, PA.
(70) Orbulescu, J.; Mullins, O. C.; Leblanc, R. M. Surface chemistry and spectroscopy of UG8 asphaltene Langmuir film, part 1. *Langmuir* **2010**, *26* (19), 15257−15264.
(71) Orbulescu, J.; Mullins, O. C.; Leblanc, R. M. Surface chemistry and spectroscopy of UG8 asphaltene Langmuir film, part 2. *Langmuir* **2010**, *26* (19), 15265−15271.
(72) Eyssautier, J.; Hénaut, I.; Levitz, P.; Espinat, D.; Barré, L. Organization of asphaltenes in a vacuum residue: A small-angle X-ray scattering (SAXS)−viscosity approach at high temperatures. *Energy Fuels* **2012**, DOI: 10.1021/ef201412j.
(73) Eyssautier, J.; Espinat, D.; Gummel, J.; Levitz, P.; Becerra, M.; Shaw, S.; Barré, L. Mesoscale organization in a physically separated vacuum residue: Comparison to asphaltenes in a simple solvent. *Energy Fuels* **2012**, DOI: 10.1021/ef201411r.
(74) Li, D. D.; Greenfield, M. L. High internal energies of proposed asphaltene strucutres. *Energy Fuels* **2011**, *25* (8), 3698−3705.
(75) Jain, S.; Ginzburg, V. V.; Jog, P.; Weinhold, J.; Srivastava, R.; Chapman, W. G. Modeling polymer-induced interactions between two grafted surfaces: Comparison between interfacial statistical associating fluid theory and self-consistent field theory. *J. Chem. Phys.* **2009**, *131*, 044908.
(76) Peczak, P.; Sirota, E. B. Impact of asphaltene nanoaggregation on heavy-hydrocarbon phase behavior. *Proceedings of the Petrophase 12th International Conference on Petroleum Phase Behavior and Fouling*; London, U.K., July 10−14, 2011
(77) Buckley, J. S.; Wang, X.; Creek, J. L. Solubility of the least-soluble asphaltenes. In *Asphaltenes, Heavy Oils and Petroleomics*; Mullins, O. C., Sheu, E. Y., Hammami, A., Marshall, A. G., Eds.; Springer: New York, 2007; pp 401−428.
(78) Buckley, J. S.; Hirasaki, G. J.; Liu, Y.; Von Drasek, S.; Wang, J. X.; Gill, B. S. Asphaltene precipitation and solvent properties of crude oils. *Pet. Sci. Technol.* **1998**, *16*, 251−285.
(79) Freed, D.; Mullins, O. C.; Zuo, J. Asphaltene gradients in the presence of GOR gradients. *Energy Fuels* **2010**, *24* (7), 3942−3949.
(80) Zuo, J. Y.; Elshahawi, H.; Mullins, O. C.; Dong, C.; Zhang, D.; Jia, N.; Zhao, H. Asphaltene gradients and tar mat formation in reservoirs under active gas charging. *Fluid Phase Equilib.* **2012**, *315*, 91−98.
(81) Zuo, J. Y.; Mullins, O. C.; Mishra, V.; Garcia, G.; Dong, C.; Zhang, D.; Pang, J. Asphaltene grading, flow assurance and tar mats in oil reservoirs. *Energy Fuels* **2012**, *26* (3), 1670−1680.
(82) *The Physics of Reservoir Fluids: Discovery through Downhole Fluid Analysis*; Mullins, O. C., Ed.; Schlumberger Press: Houston, TX, 2008.
(83) Zuo, J. Y.; Elshahawi, H.; Dong, C.; Latifzai, A. S.; Zhang, D.; Mullins, O. C. DFA assessment of connectivity for active gas charging reservoirs using DFA asphaltene gradients. *Proceedings of the Annual Technical Conference and Exhibition (ATCE)*; Golden, CO, Oct 30−Nov 2, 2011; SPE 145438.
(84) Pfeiffer, T.; Reza, Z.; Schechter, D. S.; McCain, W. D.; Mullins, O. C. Determination of fluid composition equilibrium under consideration of asphaltenes—A substantially superior way to assess reservoir connectivity than formation pressure surveys; *Proceedings of the Annual Technical Conference and Exhibition (ATCE)*; Golden, CO, Oct 30−Nov 2, 2011; SPE 145609.
(85) Mullins, O. C.; Zuo, J. Y.; Seifert, D. J.; Zeybek, M.; Elshahawi, H.; Nagarajan, N.; Maqbool, T.; Weinheber, P.; Dong, C.; Barré, L.; Pomerantz, A. E.; Zare, R. N. Asphaltene clusters, reservoir heavy oil gradients, and tar mat formation. *Proceedings of the Petrophase 13th International Conference on Petroleum Phase Behavior and Fouling*; St. Petersburg Beach, FL, June 10−15, 2012; accepted abstract.
(86) Elshahawi, H.; Latifzai, A. S.; Dong, C.; Zuo, J. Y.; Mullins, O. C. Understanding reservoir architecture using downhole fluid analysis and asphaltene science. *Proceedings of the Society of Petrophysicists and Well Log Analysts (SPWLA) 52nd Annual Logging Symposium*; Colorado Springs, CO, May 14−18, 2011.

(87) Panuganti, S. R.; Vargus, F. M.; Gonzalez, D. L.; Karup, A. S.; Chapman, W. G. PC-SAFT characterization of crude oils and modeling asphaltene phase behavior. *Fuel* **2012**, *93*, 658−663.
(88) Kurup, A. S.; Vargas, F. M.; Wang, J.; Buckley, J.; Creek, J. L.; Subramani, H. J.; Chapman, W. G. Development and application of an asphaltene deposition tool (ADEPT) for well bores. *Energy Fuels* **2011**, *25*, 4506−4516.
(89) Maqbool, T.; Balgoa, A. T.; Fogler, H. S. Revisiting asphaltene precipitation from crude oils: A case of neglected kinetic effects. *Energy Fuels* **2009**, *23*, 3681−3686.
(90) Maqbool, T.; Raha, S.; Hoepfner, M. P.; Fogler, H. S. Modeling the aggregation of asphaltene nanoaggregates in crude oil−precipitant systems. *Energy Fuels* **2011**, *25*, 1585−1596.